

Extremal Domain Translation with Neural Optimal Transport

Milena Gazdieva^{*1} Alexander Korotin^{*1,2} Daniil Selikhanovych¹ Evgeny Burnaev^{1,2}

Abstract

We propose the extremal transport (ET) which is a mathematical formalization of the theoretically best possible unpaired translation between a pair of domains w.r.t. the given similarity function. Inspired by the recent advances in neural optimal transport (OT), we propose a scalable algorithm to approximate ET maps as a limit of partial OT maps. We test our algorithm on toy examples and on the unpaired image-to-image translation task.

1. Introduction

The **unpaired** translation task (Zhu et al., 2017, Fig. 2) is to find a map $x \mapsto T(x)$, usually a neural network, which transports the samples x from the given source domain to the target domain. The key challenge here is that the **correspondence** between available data samples x from the source and y from target domains **is not given**. Thus, the task is ill-posed as there might exist multiple suitable T .

When solving the task, many methods regularize the translated samples $T(x)$ to inherit specific attributes of the respective input samples x . In the popular unpaired translation (Zhu et al., 2017, Fig. 9) and enhancement (Yuan et al., 2018, Equation 3) tasks for images, it is common to use additional *unsupervised* identity losses, e.g., $\|T(x) - x\|_1$, to make the translated output $T(x)$ be similar to the input images x . The same applies, e.g., to audio translation (Mathur et al., 2019). Therefore, the learning objectives of such methods usually have two following components:

1. **Domain loss** (main) enforcing the translated sample $T(x)$ to look like the samples y from the target domain.
2. **Similarity loss** (regularizer, *optional*) stimulating the translated $T(x)$ to inherit certain attributes of input x .

A question arises: can one obtain the **maximal** similarity of $T(x)$ to x but still ensure that $T(x)$ is indeed from the target domain? A straightforward "yes, just increase the weight of the similarity loss" may work but only to a limited extent. We demonstrate this in Appendix C.

^{*}Equal contribution ¹Skolkovo Institute of Science and Technology, Moscow, Russia ²Artificial Intelligence Research Institute, Moscow, Russia. Correspondence to: Milena Gazdieva <milena.gazdieva@skoltech.ru>.



(a) Handbag \rightarrow shoes (128×128).



(b) Celeba (female) \rightarrow anime (64×64).

Figure 1: (Nearly) extremal transport with our Algorithm 1. Higher w yields bigger similarity of x and $T(x)$ in ℓ^2 .

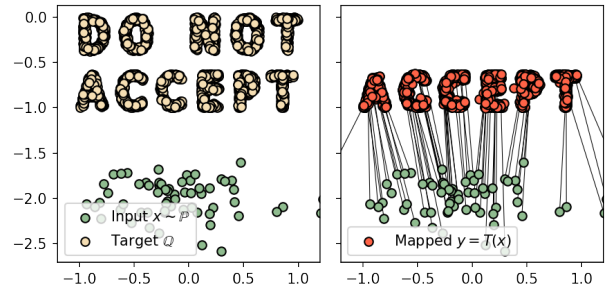


Figure 2: Learned transport map ($w = 2$) in 'Accept' task.

Contributions. In this paper, we propose the *extremal transport* (ET, §3.1) which is a rigorous mathematical task formulation describing the theoretically best possible unpaired domain translation w.r.t. the given similarity function. We explicitly characterize ET maps and plans by establishing an intuitive connection to the nearest neighbors (NN). We show that ET maps can be learned as a limit (§3.3) of specific partial optimal transport (OT) problem which we call *incomplete transport* (IT, §3.2). For IT, we derive the duality formula yielding an efficient computational algorithm (§3.4). We test our proposed algorithm on toy 2D examples and the unpaired image-to-image translation (§5).

Notation. We consider *compact* Polish spaces $(\mathcal{X}, \|\cdot\|_{\mathcal{X}})$, $(\mathcal{Y}, \|\cdot\|_{\mathcal{Y}})$ and use $\mathcal{P}(\mathcal{X})$, $\mathcal{P}(\mathcal{Y})$ to denote the sets of Radon probability measures on them. We use $\mathcal{M}_+(\mathcal{X}) \subset \mathcal{M}(\mathcal{X})$ to denote the sets of finite non-negative and finite signed (Radon) measures on \mathcal{X} , respectively. They both contain $\mathcal{P}(\mathcal{X})$ as a subset. For a non-negative $\mu \in \mathcal{M}_+(\mathcal{X})$, its support is denoted by $\text{Supp}(\mu) \subset \mathcal{X}$. It is a closed set consisting of all points $x \in \mathcal{X}$ for which every open neighbourhood $A \ni x$ satisfies $\mu(A) > 0$. We use $\mathcal{C}(\mathcal{X})$ to denote the set of continuous functions $\mathcal{X} \rightarrow \mathbb{R}$ equipped with $\|\cdot\|_{\infty}$ norm. Its dual space is $\mathcal{M}(\mathcal{X})$ equipped with the $\|\cdot\|_1$ norm. A sequence $\mu_1, \mu_2, \dots \in \mathcal{M}(\mathcal{X})$ is said to be weakly-* converging to $\mu^* \in \mathcal{M}(\mathcal{X})$ if for every $f \in \mathcal{C}(\mathcal{X})$ it holds that $\lim_{n \rightarrow \infty} \int_{\mathcal{X}} f(x) d\mu_n(x) = \int_{\mathcal{X}} f(x) d\mu^*(x)$. For a probability measure $\pi \in \mathcal{P}(\mathcal{X} \times \mathcal{Y})$, we use $\pi_x \in \mathcal{P}(\mathcal{X})$ and $\pi_y \in \mathcal{P}(\mathcal{Y})$ to denote its projections onto \mathcal{X} , \mathcal{Y} , respectively. Disintegration of π yields $d\pi(x, y) = d\pi_x(x) d\pi(y|x)$, where $\pi(y|x)$ denotes the conditional distribution of $y \in \mathcal{Y}$ for a given $x \in \mathcal{X}$. For $\mu, \nu \in \mathcal{M}(\mathcal{Y})$, we write $\mu \leq \nu$ if for all measurable $A \subset \mathcal{Y}$ it holds that $\mu(A) \leq \nu(A)$. For a measurable map $T : \mathcal{X} \rightarrow \mathcal{Y}$, we use $T_{\#}$ to denote the associated pushforward operator $\mathcal{P}(\mathcal{X}) \rightarrow \mathcal{P}(\mathcal{Y})$.

2. Background on Optimal Transport

In this section, we give an overview of the OT theory concepts related to our paper. For details on OT, we refer to (Santambrogio, 2015; Villani, 2008; Peyré et al., 2019), partial OT - (Figalli, 2010; Caffarelli & McCann, 2010).

Let $c : \mathcal{X} \times \mathcal{Y} \rightarrow \mathbb{R}$ be a continuous cost function.

Standard OT formulation. For $\mathbb{P} \in \mathcal{P}(\mathcal{X})$, $\mathbb{Q} \in \mathcal{P}(\mathcal{Y})$, the OT cost between them is given by (Fig. 3)

$$\text{Cost}(\mathbb{P}, \mathbb{Q}) \stackrel{\text{def}}{=} \inf_{T: \mathbb{P} \rightarrow \mathbb{Q}} \int_{\mathcal{X}} c(x, T(x)) d\mathbb{P}(x), \quad (1)$$

where inf is taken over measurable $T : \mathcal{X} \rightarrow \mathcal{Y}$ pushing \mathbb{P} to \mathbb{Q} (transport maps). Problem (1) is called the *Monge's OT problem*, and its minimizer T^* is called an *OT map*.

In some cases, there may be no minimizer T^* of (1). Therefore, it is common to consider *Kantorovich's* relaxation:

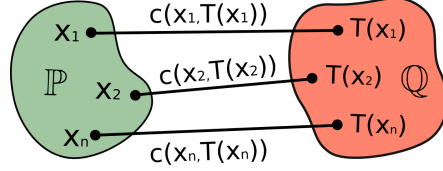


Figure 3: Monge's optimal transport formulation.

$$\text{Cost}(\mathbb{P}, \mathbb{Q}) \stackrel{\text{def}}{=} \inf_{\pi \in \Pi(\mathbb{P}, \mathbb{Q})} \int_{\mathcal{X} \times \mathcal{Y}} c(x, y) d\pi(x, y), \quad (2)$$

where inf is taken over $\pi \in \mathcal{P}(\mathcal{X} \times \mathcal{Y})$ satisfying $\pi_x = \mathbb{P}$ and $\pi_y = \mathbb{Q}$, respectively. A minimizer $\pi^* \in \Pi(\mathbb{P}, \mathbb{Q})$ in (2) always exists and is called an *OT plan*. To provide an intuition behind (2), we disintegrate $d\pi(x, y) = d\pi_x(x) d\pi(y|x)$:

$$\inf_{\pi \in \Pi(\mathbb{P}, \mathbb{Q})} \int_{\mathcal{X}} \left\{ \int_{\mathcal{Y}} c(x, y) d\pi(y|x) \right\} \underbrace{d\mathbb{P}(x)}_{=d\pi_x(x)}, \quad (3)$$

i.e., (2) can be viewed as an extension of (1), which allows to *split* the mass of input points $x \sim \mathbb{P}$, see Fig. 4. With mild assumptions on \mathbb{P} , \mathbb{Q} , the OT cost value (2) coincides with (1), see (Santambrogio, 2015, Theorem 1.33).

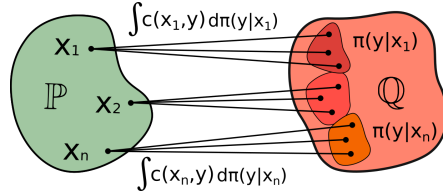


Figure 4: Kantorovich's optimal transport formulation.

Partial OT formulation. Let $w_0, w_1 \geq m \geq 0$. We consider

$$\inf_{\substack{m\pi_x \leq w_0\mathbb{P} \\ m\pi_y \leq w_1\mathbb{Q}}} \int_{\mathcal{X} \times \mathcal{Y}} c(x, y) d[m\pi](x, y), \quad (4)$$

where inf is taken over $\pi \in \mathcal{P}(\mathcal{X} \times \mathcal{Y})$ satisfying the inequality constraints $m\pi_x \leq w_0\mathbb{P}$ and $m\pi_y \leq w_1\mathbb{Q}$. Minimizers π^* of (4) are called *partial OT plans* (Fig. 5).

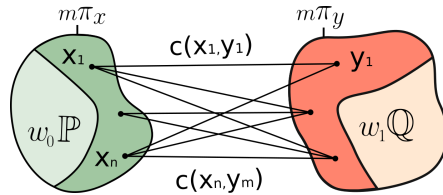


Figure 5: Partial optimal transport formulation.

Here the inputs are two measures $w_0\mathbb{P}$ and $w_1\mathbb{Q}$ with masses w_0 and w_1 . Intuitively, we need to match a $\frac{m}{w_0}$ -th fraction $m\pi_x$ of the first measure $w_0\mathbb{P}$ with a $\frac{m}{w_1}$ -th fraction $m\pi_y$ of the second measure $w_1\mathbb{Q}$ (Fig. 5); choosing π_x, π_y is also a part of this problem. The key difference from problem (4)

is that the constraints are *inequalities*. In the particular case $m = w_0 = w_1$, problem (4) reduces to (2) as the inequality constraints can be replaced by equalities.

3. Main Results

First, we formulate the extremal transport (ET) problem (§3.1). Next, we prove that ET maps can be recovered as a limit of incomplete transport (IT) maps (§3.2, 3.3). Then we propose an algorithm to solve the IT problem (§3.4). We provide the proofs for all the theorems in Appendix E.

3.1. Extremal Transport Problem

Popular unpaired translation methods, e.g., (Zhu et al., 2017, §3.1) and (Huang et al., 2018, §3), de-facto assume that available samples x, y from the input and output domains come from the data distributions $\mathbb{P}, \mathbb{Q} \in \mathcal{P}(\mathcal{X}), \mathcal{P}(\mathcal{Y})$. As a result, in their optimization objectives, the *domain loss* compares the translated $T(x) \sim T\#\mathbb{P}$ and target samples $y \sim \mathbb{Q}$ by using a metric for comparing *probability measures*, e.g., GAN loss (Goodfellow et al., 2014). Thus, the target *domain* is identified with the probability measure \mathbb{Q} .

We pick a different approach to define what the *domain* is. We still assume that the available data comes from data distributions, i.e., $x \sim \mathbb{P}, y \sim \mathbb{Q} \in \mathcal{P}(\mathcal{Y})$. However, we say that the target domain is the part of \mathcal{Y} where the probability mass of \mathbb{Q} lives. Namely, it is $\text{Supp}(\mathbb{Q}) \subset \mathcal{Y}$. We say that a map T translates the domains if $\text{Supp}(T\#\mathbb{P}) \subset \text{Supp}(\mathbb{Q})$. This is a weaker requirement than the usual $T\#\mathbb{P} = \mathbb{Q}$.

Assume that $c(x, y)$ is a function estimating the dissimilarity between x, y . We would like to pick $T(x) \in \text{Supp}(\mathbb{Q})$ which is *maximally* similar to x in terms of $c(x, y)$. This preference of T can be formalized as follows:

$$\text{Cost}_\infty(\mathbb{P}, \mathbb{Q}) \stackrel{\text{def}}{=} \inf_{\substack{\text{Supp}(T\#\mathbb{P}) \subset \text{Supp}(\mathbb{Q}) \\ T: \mathcal{X} \rightarrow \mathcal{Y}}} \int_{\mathcal{X}} c(x, T(x)) d\mathbb{P}(x), \quad (5)$$

where the inf is taken over measurable $T: \mathcal{X} \rightarrow \mathcal{Y}$ which map the probability mass of \mathbb{P} to $\text{Supp}(\mathbb{Q})$. We say that (5) is the (Monge's) *extremal transport* (ET) problem.

Problem (5) is **atypical** for the common OT framework. For example, the usual measure-preserving constraint $T\#\mathbb{P} = \mathbb{Q}$ in (1) is replaced with $\text{Supp}(T\#\mathbb{P}) \subset \text{Supp}(\mathbb{Q})$ which is more tricky. Importantly, measure \mathbb{Q} can be replaced with any other $\mathbb{Q}' \in \mathcal{P}(\mathcal{Y})$ with the same support yielding the same inf. Below we analyse the minimizers T^* of (5).

We define $c^*(x) \stackrel{\text{def}}{=} \min_{y \in \text{Supp}(\mathbb{Q})} c(x, y)$. Here the min is indeed attained (for all $x \in \mathcal{X}$) because $c(x, y)$ is continuous and $\text{Supp}(\mathbb{Q}) \subset \mathcal{Y}$ is a compact set. The value $c^*(x)$ can be understood as the *lowest* possible transport cost when mapping the mass of point x to the support of \mathbb{Q} .

For any admissible T in (5), it holds (\mathbb{P} -almost surely):

$$c^*(x) = \min_{y \in \text{Supp}(\mathbb{Q})} c(x, y) \leq c(x, T(x)). \quad (6)$$

Proposition 1 (Continuity of c^*). *It holds that $c^* \in \mathcal{C}(\mathcal{X})$.*

As a consequence of Proposition 1, we see that c^* is measurable. We integrate (6) w.r.t. $x \sim \mathbb{P}$ and take inf over all feasible T . This yields a lower bound on $\text{Cost}_\infty(\mathbb{P}, \mathbb{Q})$:

$$\int_{\mathcal{X}} c^*(x) d\mathbb{P}(x) \leq \overbrace{\inf_{\substack{\text{Supp}(T\#\mathbb{P}) \subset \text{Supp}(\mathbb{Q}) \\ T: \mathcal{X} \rightarrow \mathcal{Y}}} \int_{\mathcal{X}} c(x, T(x)) d\mathbb{P}(x)}^{\text{Cost}_\infty(\mathbb{P}, \mathbb{Q})}. \quad (7)$$

There exists admissible T making (7) the equality. Indeed, let $\text{NN}(x) \stackrel{\text{def}}{=} \{y \in \text{Supp}(\mathbb{Q}) \text{ s.t. } c(x, y) = c^*(x)\}$ be the set of points y which attain min in the definition of c^* . These points are the closest to x points in \mathbb{Q} w.r.t. the cost $c(x, y)$. We call them the *nearest neighbors* of x . From this perspective, we see that (7) turns to equality if and only if $T(x) \in \text{NN}(x)$ holds for \mathbb{P} -almost all $x \in \mathcal{X}$, i.e., T maps points $x \sim \mathbb{P}$ to their nearest neighbors in $\text{Supp}(\mathbb{Q})$. We need to make sure that such *measurable* T exists (Fig. 6).

Theorem 1 (Existence of ET maps). *There exists at least one measurable map $T^*: \mathcal{X} \rightarrow \mathcal{Y}$ minimizing (5). For \mathbb{P} -almost all $x \in \mathcal{X}$ it holds that $T^*(x) \in \text{NN}(x)$. Besides,*

$$\text{Cost}_\infty(\mathbb{P}, \mathbb{Q}) = \int_{\mathcal{X}} c^*(x) d\mathbb{P}(x).$$

We say that $\text{Cost}_\infty(\mathbb{P}, \mathbb{Q})$ is the *extremal cost* because one can not obtain smaller cost when moving the mass of \mathbb{P} to $\text{Supp}(\mathbb{Q})$. In turn, we say that minimizers T^* are *ET maps*.

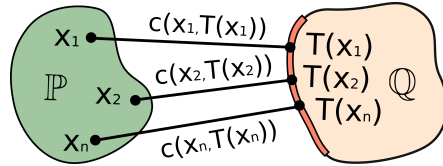


Figure 6: Monge's extremal transport formulation.

One may extend the ET problem (8) in the Kantorovich's manner by allowing the mass splitting and stochastic plans:

$$\text{Cost}_\infty(\mathbb{P}, \mathbb{Q}) \stackrel{\text{def}}{=} \inf_{\pi \in \Pi^\infty(\mathbb{P}, \mathbb{Q})} \int_{\mathcal{X} \times \mathcal{Y}} c(x, y) d\pi(x, y), \quad (8)$$

where $\Pi^\infty(\mathbb{P}, \mathbb{Q})$ are probability measures $\pi \in \mathcal{P}(\mathcal{X} \times \mathcal{Y})$ satisfying $\pi_x = \mathbb{P}$ and $\text{Supp}(\pi_y) \subset \text{Supp}(\mathbb{Q})$.

To understand the structure of minimizers in (8), it is more convenient to disintegrate $d\pi(x, y) = d\pi(y|x) d\pi_x(x)$:

$$\text{Cost}_\infty(\mathbb{P}, \mathbb{Q}) = \inf_{\pi \in \Pi^\infty(\mathbb{P}, \mathbb{Q})} \int_{\mathcal{X}} \int_{\mathcal{Y}} c(x, y) d\pi(y|x) \underbrace{d\mathbb{P}(x)}_{=d\pi_x(x)}. \quad (9)$$

Thus, computing (8) boils down to computing a family of conditional measures $\pi(\cdot|x)$ minimizing (8). As in (7), for any $\pi \in \Pi^\infty(\mathbb{P}, \mathbb{Q})$, it holds (for \mathbb{P} -almost all $x \in \mathcal{X}$) that

$$c^*(x) = \min_{y \in \text{Supp}(\mathbb{Q})} c(x, y) \leq \int_{\mathcal{Y}} c(x, y) d\pi(y|x) \quad (10)$$

because π redistributes the mass of \mathbb{P} to $\text{Supp}(\mathbb{Q})$. This also means that $\int_{\mathcal{X}} c^*(x) d\mathbb{P}(x)$ is a lower bound for (8). In particular, the bound is tight for $\pi^*(y|x) = \delta_{T^*(x)}$, where T^* is the ET map from our Theorem 1. Therefore, the value (8) is the same as (5) but possibly admits more minimizers. We call the minimizers π^* of (8) the *ET plans* (Fig. 7).

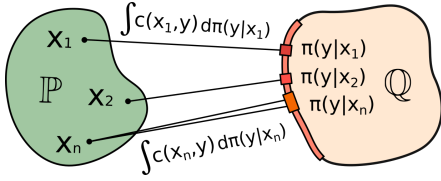


Figure 7: Kantorovich's extremal transport formulation.

From (10) and the definition of $\text{NN}(x)$, we see that minimizers π^* are the plans for which $\pi^*(y|x)$ redistributes the mass of x among the nearest neighbors $y \in \text{NN}(x)$ of x (for \mathbb{P} -almost all $x \in \mathcal{X}$). As a result, $\pi^*(y|x)$ can be viewed as a *stochastic nearest neighbor assignment* between the probability mass of \mathbb{P} and the support of \mathbb{Q} .

3.2. Incomplete Transport Problem

In practice, solving extremal problem (5) is challenging because it is hard to enforce $\text{Supp}(T\# \mathbb{P}) \subset \text{Supp}(\mathbb{Q})$. To avoid enforcing this constraint, we soften it and consider the following problem with finite parameter $w \geq 1$:

$$\text{Cost}_w(\mathbb{P}, \mathbb{Q}) \stackrel{\text{def}}{=} \inf_{T\# \mathbb{P} \leq w\mathbb{Q}} \int_{\mathcal{X}} c(x, T(x)) d\mathbb{P}(x). \quad (11)$$

We call (11) Monge's *incomplete transport* (IT) problem (Fig. 8). With the increase of w , admissible maps T obtain more ways to redistribute the mass of \mathbb{P} among $\text{Supp}(\mathbb{Q})$. Informally, when $w \rightarrow \infty$, the constraint $T\# \mathbb{P} \leq w\mathbb{Q}$ in (11) tends to the constraint $\text{Supp}(T\# \mathbb{P}) \subset \text{Supp}(\mathbb{Q})$ in (5), i.e., (11) itself tends to ET problem (5). We will formalize this statement a few paragraphs later (in §3.3).

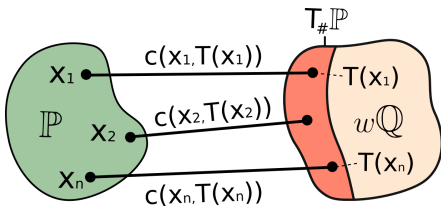


Figure 8: Monge's incomplete transport formulation.

As in (1), problem (11) may have no minimizer T^* or even may have the empty feasible set. Therefore, it is natural to relax problem (11) in the Kantorovich's manner:

$$\text{Cost}_w(\mathbb{P}, \mathbb{Q}) \stackrel{\text{def}}{=} \inf_{\pi \in \Pi^w(\mathbb{P}, \mathbb{Q})} \int_{\mathcal{X} \times \mathcal{Y}} c(x, y) d\pi(x, y), \quad (12)$$

where the inf is taken over the set $\Pi^w(\mathbb{P}, \mathbb{Q})$ of probability measures $\pi \in \mathcal{P}(\mathcal{X} \times \mathcal{Y})$ whose first marginal is $\pi_x = \mathbb{P}$, and the second marginal satisfies $\pi_y \leq w\mathbb{Q}$ (Fig. 9).

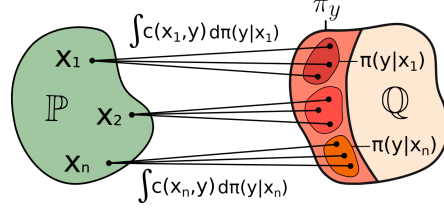


Figure 9: Kantorovich's incomplete transport formulation.

We note that IT problem (12) is a special case of partial OT (4) with $w_0 = m = 1$ and $w_1 = w$. In (12), one may actually replace inf with min, see our proposition below.

Proposition 2. (*Existence of IT plans*). *Problem (12) admits at least one minimizer $\pi^* \in \Pi^w(\mathbb{P}, \mathbb{Q})$.*

We say that minimizers of (12) are *IT plans*. In the general case, Kantorovich's *IT cost* (12) always lower bounds Monge's counterpart (11). Below we show that they coincide in the practically most interesting Euclidean case.

Proposition 3 (Equivalence of Monge's and Kantorovich's IT costs). *Let $\mathcal{X}, \mathcal{Y} \subset \mathbb{R}^D$ be two compact sets. Let $\mathbb{P} \in \mathcal{P}(\mathcal{X})$ be atomless and $\mathbb{Q} \in \mathcal{P}(\mathcal{Y})$. Then Monge's (11) and Kantorovich's (12) IT costs coincide.*

However, it is not guaranteed that inf in Monge's problem (11) is attained even in the Euclidean case. Still for general Polish spaces \mathcal{X}, \mathcal{Y} it is clear that if there exists a deterministic IT plan in Kantorovich's problem (12) of the form $\pi^* = [\text{id}_{\mathcal{X}}, T^*]$, then T^* is an IT map in (11), and the IT Monge's (11) and Kantorovich's (12) costs coincide.

Henceforth, for simplicity, we assume that $\mathcal{X}, \mathcal{Y}, c, \mathbb{P}, \mathbb{Q}$ are such that (11) and (12) coincide, e.g., those from Prop. 3.

IT problem (12) can be viewed as an interpolation between OT (2) and ET problems (8). Indeed, when $w = 1$, the constraint $\pi_y \leq \mathbb{Q}$ is equivalent to $\pi_y = \mathbb{Q}$ as there is only one *probability* measure which is $\leq \mathbb{Q}$, and it is \mathbb{Q} itself. Thus, IT (12) with $w = 1$ coincides with OT (2). In the next section, we show that for $w \rightarrow \infty$ one recovers ET from IT.

3.3. Link between Incomplete and Extremal Transport

Now we connect incomplete (12) and extremal (8) tasks.

Theorem 2. (IT costs converge to the ET cost when $w \rightarrow \infty$) *Function $w \mapsto \text{Cost}_w(\mathbb{P}, \mathbb{Q})$ is convex, non-increasing in $w \in [1, +\infty)$ and*

$$\lim_{w \rightarrow \infty} \text{Cost}_w(\mathbb{P}, \mathbb{Q}) = \text{Cost}_\infty(\mathbb{P}, \mathbb{Q}).$$

A natural subsequent question here is whether IT plans in (12) converge to ET plans (8) when $w \rightarrow \infty$. Our following result sheds the light on this question.

Theorem 3. (IT plans converge to ET plans when $w \rightarrow \infty$). *Consider $w_1, w_2, w_3, \dots \geq 1$ satisfying $\lim_{n \rightarrow \infty} w_n = \infty$. Let $\pi^{w_n} \in \Pi^{w_n}(\mathbb{P}, \mathbb{Q})$ be a sequence of IT plans solving (12) with $w = w_n$, respectively. Then it has a (weakly-*) converging sub-sequence. Every such sub-sequence of IT plans converges to an ET plan $\pi^* \in \Pi^\infty(\mathbb{P}, \mathbb{Q})$.*

Providing a stronger convergence result here is challenging because, in general, there may be sub-sequences converging to different ET plans $\pi^* \in \Pi^\infty(\mathbb{P}, \mathbb{Q})$. We leave this interesting theoretical question open for future studies.

Our Theorems 2 and 3 suggest that to obtain a fine approximation of an ET plan ($w = \infty$), one may use an IT plan for sufficiently large finite w . Below we develop a neural algorithm to compute IT plans.

3.4. Computational Algorithm for Incomplete Transport

To begin with, for IT (12), we derive the dual problem.

Theorem 4. (Dual problem for IT) *It holds*

$$\text{Cost}_w(\mathbb{P}, \mathbb{Q}) = \max_{f \leq 0} \int_{\mathcal{X}} f^c(x) d\mathbb{P}(x) + w \int_{\mathcal{Y}} f(y) d\mathbb{Q}(y), \quad (13)$$

where the max is taken over non-positive $f \in \mathcal{C}(\mathcal{Y})$ and $f^c(x) \stackrel{\text{def}}{=} \min_{y \in \mathcal{Y}} \{c(x, y) - f(y)\}$ is the c -transform of f .

We call the function f *potential*. In the definition of f^c , min is attained because c, f are continuous and \mathcal{Y} is compact.

The difference of formula (13) from usual c -transform-based duality formulas for OT (2), see (Santambrogio, 2015, §1.2), (Villani, 2008, §5), is that f is required to be non-positive and the second term is multiplied by $w \geq 1$.

We rewrite the term $\int_{\mathcal{X}} f^c(x) d\mathbb{P}(x)$ in (13):

$$\begin{aligned} \int_{\mathcal{X}} f^c(x) d\mathbb{P}(x) &= \int_{\mathcal{X}} \min_{y \in \mathcal{Y}} \{c(x, y) - f(y)\} d\mathbb{P}(x) = \\ &= \inf_{T: \mathcal{X} \rightarrow \mathcal{Y}} \int_{\mathcal{X}} \{c(x, T(x)) - f(y)\} d\mathbb{P}(x). \end{aligned} \quad (14)$$

Here we use the interchange between the integral and inf (Rockafellar, 1976, Theorem 3A); in (14) the inf is taken

over measurable maps. Since $(x, y) \mapsto c(x, y) - f(y)$ is a continuous function on a compact set, it admits a measurable selection $T(x) \in \arg \min_{y \in \mathcal{Y}} \{c(x, y) - f(y)\}$ minimizing (14), see (Aliprantis & Border, 2006, Theorem 18.19). Thus, inf can be replaced by min. We combine (14) and (13) and obtain an equivalent saddle point problem:

$$\text{Cost}_w(\mathbb{P}, \mathbb{Q}) = \max_{f \leq 0} \min_{T: \mathcal{X} \rightarrow \mathcal{Y}} \mathcal{L}(f, T), \quad (15)$$

where the functional $\mathcal{L}(f, T)$ is defined by

$$\begin{aligned} \mathcal{L}(f, T) &\stackrel{\text{def}}{=} \int_{\mathcal{X}} c(x, T(x)) d\mathbb{P}(x) - \\ &- \int_{\mathcal{X}} f(T(x)) d\mathbb{P}(x) + w \int_{\mathcal{Y}} f(y) d\mathbb{Q}(y). \end{aligned} \quad (16)$$

Functional $\mathcal{L}(f, T)$ can be viewed as a Lagrangian with $f \leq 0$ being a multiplier for the constraint $T\#\mathbb{P} - w\mathbb{Q} \leq 0$. By solving (15), one may obtain IT maps.

Theorem 5 (IT maps are contained in optimal saddle points). *Let f^* be any maximizer in (13). If $\pi^* \in \Pi^w(\mathbb{P}, \mathbb{Q})$ is a deterministic IT plan, i.e., it solves (12) and has the form $\pi^* = [\text{id}_{\mathcal{X}}, T^*]\#\mathbb{P}$ for some measurable $T^*: \mathcal{X} \rightarrow \mathcal{Y}$, then*

$$T^* \in \arg \min_{T: \mathcal{X} \rightarrow \mathcal{Y}} \mathcal{L}(f^*, T).$$

Our Theorem 5 states that in *some* optimal saddle points (f^*, T^*) of (15) it holds that T^* is the IT map between \mathbb{P}, \mathbb{Q} . In general, the $\arg \inf_T$ set for an optimal f^* might contain not only IT maps T^* , but other functions as well (*fake solutions*), see limitations in Appendix A.

We solve the optimization problem (15) by approximating the map T and potential f with neural networks T_θ and f_ψ , respectively. To make f_ψ non-positive, we use $x \mapsto -|x|$ as the last layer. The nets are trained using random batches from \mathbb{P}, \mathbb{Q} and stochastic gradient ascent-descent. We detail the optimization procedure in Algorithm 1.

4. Related work

OT in generative models. A popular way to apply OT in generative models is to use the **OT cost** as the loss function to update the generator (Arjovsky et al., 2017; Gulrajani et al., 2017; Genevay et al., 2018), see (Korotin et al., 2022a) for a survey. These methods are *not relevant* to our study as they do not learn an OT map but only compute the OT cost.

Recent works (Korotin et al., 2022c;b; Rout et al., 2021; Fan et al., 2021; Asadulaev et al., 2022; Gazdieva et al., 2022; Gushchin et al., 2022) are the most related to our study. These papers show the possibility to learn the **OT maps** (or plans) via solving saddle point optimization problems derived from the standard c -transform-based duality

Algorithm 1: Procedure to compute the IT map between \mathbb{P} and \mathbb{Q} for transport cost $c(x, y)$ and weight w .

Input : distributions \mathbb{P}, \mathbb{Q} accessible by samples;
 mapper $T_\theta : \mathcal{X} \rightarrow \mathcal{Y}$; potential $f_\psi : \mathcal{X} \rightarrow \mathbb{R}_-$;
 transport cost $c : \mathcal{X} \times \mathcal{Y} \rightarrow \mathbb{R}$; weight $w \geq 1$;
 number K_T of inner iterations;

Output : approximate IT map $(T_\theta)_\# \mathbb{P} \leq w\mathbb{Q}$;

repeat

 Sample batches $X \sim \mathbb{P}, Y \sim \mathbb{Q}$;
 $\mathcal{L}_f \leftarrow w \cdot \frac{1}{|Y|} \sum_{y \in Y} f_\psi(y) - \frac{1}{|X|} \sum_{x \in X} f_\psi(T_\theta(x))$;
 Update ψ by using $\frac{\partial \mathcal{L}_f}{\partial \psi}$ to maximize \mathcal{L}_f ;
 for $k_T = 1, 2, \dots, K_T$ **do**
 Sample batch $X \sim \mathbb{P}$;
 $\mathcal{L}_T \leftarrow \frac{1}{|X|} \sum_{x \in X} [c(x, T_\theta(x)) - f_\psi(T_\theta(x))]$;
 Update θ by using $\frac{\partial \mathcal{L}_T}{\partial \theta}$ to minimize \mathcal{L}_T ;

until not converged;

formulas for OT. The underlying principle of our objective (15) is analogous to theirs. The key **difference** is that they consider OT problems (1), (2) and enforce the *equality* constraints, e.g., $T_\# \mathbb{P} = \mathbb{Q}$, while our approach enforces the *inequality* constraint $T_\# \mathbb{P} \leq w\mathbb{Q}$ allowing to *partially* align the measures. *We provide a detailed discussion of relation with these works as well as with the fundamental OT (2) and partial OT (4) literature* (Figalli, 2010; Caffarelli & McCann, 2010; Santambrogio, 2015) in Appendix E.

For completeness, we also mention other existing neural OT methods (Genevay et al., 2016; Seguy et al., 2017; Makkua et al., 2019; Daniels et al., 2021; Korotin et al., 2021a). These works are less related to our work because they either underperform compared to the above-mentioned saddle point methods, see (Korotin et al., 2021b) for evaluation, or they solve specific OT formulations, e.g., entropic OT (Peyré et al., 2019, §4), which are not relevant to our study.

The papers (Yang & Uhler, 2018; Lübeck et al., 2022; Eyring et al., 2022) are slightly more related to our work. They propose neural methods for unbalanced OT (Chizat, 2017) which can also be used to *partially* align measures. As we will see in Appendix B, UOT is hardly suitable for ET (8) as it is not easy to control how it spreads the probability mass. Besides, these methods consider OT between small-dimensional datasets or in latent spaces. It is not clear whether they scale to high-dimensions, e.g., images.

Unpaired domain translation (Alotaibi, 2020) is a generic problem which includes image super-resolution (Chen et al., 2022), inpainting (Zhang et al., 2022), style translation (Jing et al., 2019) tasks, etc. Therefore, we do not mention all of the existing approaches but focus on their common main

features instead. In many applications, it is important to preserve semantical information during the translation, e.g., the image content. In most cases, to do this it suffices to use convolutional neural networks. They preserve the image content thanks to their design which is targeted to only locally change the image (de Bézenac et al., 2021). However, in some of the tasks additional properties of the image must be kept, e.g., image colors in super-resolution. Typical approaches to such problems are based on GANs and use additional *similarity* losses, e.g., the basic CycleGAN (Zhu et al., 2017) enforces ℓ^1 similarity. Such methods are mostly related to our work. As we show in experiments, IT achieves better similarity than CycleGAN (Appendix C).

5. Evaluation

In §5.1, we provide illustrative toy 2D examples. In §5.2, we evaluate our method on the unpaired image-to-image translation task. The code is written using PyTorch framework and will be made publicly available.

Transport costs. We experiment with the quadratic cost $c(x, y) = \ell^2(x, y)$ as this cost already provides reasonable performance. We slightly abuse the notation and use ℓ^2 to denote the squared error *normalized* by the dimension.

Technical **training details** (architectures, learning rates, batch sizes, schedulers, etc.) are given in Appendix D.

5.1. Toy 2D experiments

In this section, we provide ‘Wi-Fi’ and ‘Accept’ examples in 2D to show how the choice of w affects the fraction of the target measure \mathbb{Q} to which the probability mass of the input \mathbb{P} is mapped. In both cases, measure \mathbb{P} is *Gaussian*.

In ‘Wi-Fi’ experiment (Fig. 10), target \mathbb{Q} contains 3 arcs. We provide the learned IT maps for $w \in [1, \frac{3}{2}, 3]$. The results show that by varying w it is possible to control the fraction of \mathbb{Q} to which the mass of \mathbb{P} will be mapped. In Fig. 10, we see that for $w = 1$ our IT method learns all 3 arcs. For $w = \frac{3}{2}$, it captures 2 arcs, i.e., $\approx \frac{2}{3}$ of \mathbb{Q} . For $w = 3$, it learns 1 arc which corresponds to $\approx \frac{1}{3}$ of \mathbb{Q} .

In ‘Accept’ experiment (Fig. 2), target \mathbb{Q} is a two-line text. Here we put $w = 2$ and, as expected, our method captures only one line of the text which is the closest to \mathbb{P} in ℓ^2 .

In Appendix B, we demonstrate how *other methods* perform on these ‘Wi-Fi’ and ‘Accept’ toy examples.

5.2. Unpaired Image-to-image Translation

Here we learn IT maps between different pairs of image datasets. We consider $w \in \{1, 2, 4, 8\}$ in all experiments.

Image datasets. We utilize the following publicly available datasets as \mathbb{P}, \mathbb{Q} : celebrity faces (Liu et al., 2015), aligned

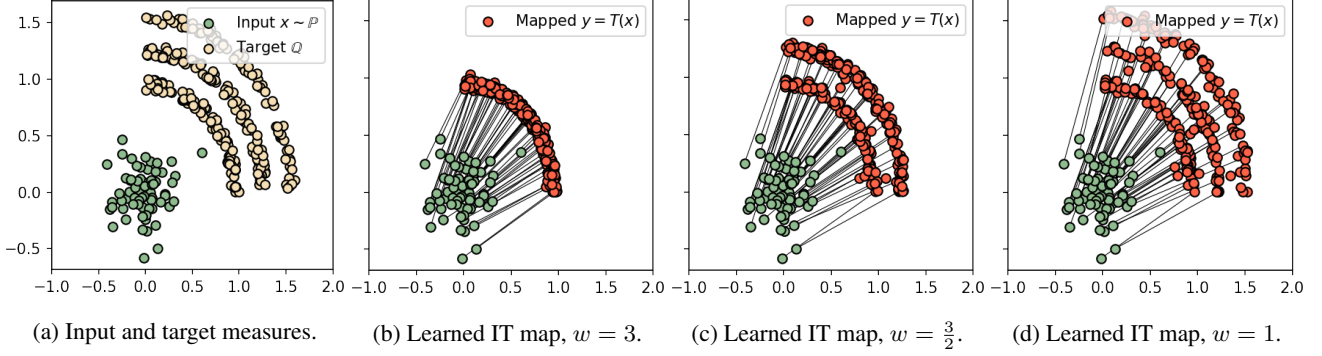
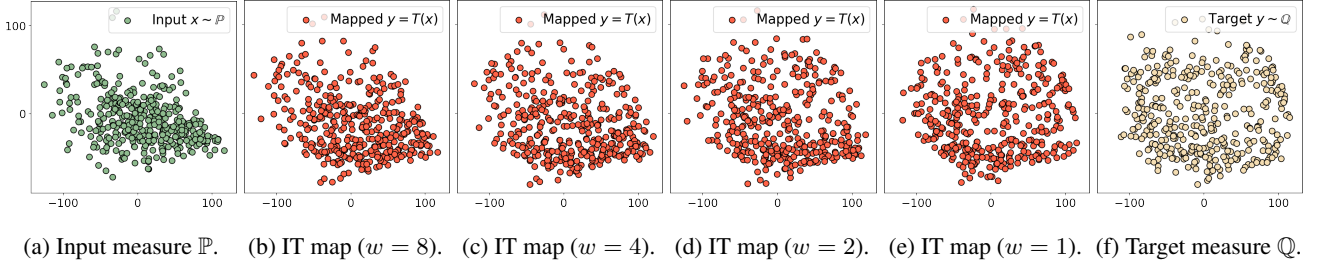


Figure 10: Incomplete transport (IT) maps learned by our Algorithm 1 in 'Wi-Fi' experiment.


 Figure 11: PCA projections of input $x \sim \mathbb{P}$, mapped $T(x) \sim T\#\mathbb{P}$ and target $y \sim \mathbb{Q}$ test samples (*handbag* \rightarrow *shoes* experiment).

anime faces¹, flickr-faces-HQ (Karras et al., 2019), comic faces², Amazon handbags from LSUN dataset (Yu et al., 2015), shoes (Yu & Grauman, 2014), textures (Cimpoi et al., 2014) and chairs from Bonn furniture styles dataset (Aggarwal et al., 2018). The sizes of datasets are from 5K to 500K samples. We work with 64×64 and 128×128 images.

Train-test split. We use 90% of each dataset for training. The remaining 10% are held for test. All the presented qualitative and quantitative results are obtained for test images.

Experimental results. Our evaluation shows that with the increase of w the images $\hat{T}(x)$ translated by our IT method become more similar to the respective inputs x w.r.t. ℓ^2 . In Table 1, we quantify this effect. Namely, we show that the test transport cost $\frac{1}{N_{\text{test}}} \sum_{n=1}^{N_{\text{test}}} c(x, \hat{T}(x))$ decreases with the increase of w which empirically verifies our Theorem 2.

We qualitatively demonstrate this effect in Fig. 1b, 1a, 13, 12 and 11. In *celeba* (female) \rightarrow *anime* (Fig. 1b), the hair and background colors of the learned anime images become closer to celebrity faces' colors with the increase of w . For example, in the 4th column of Fig. 1b, the anime hair color changes from green to brown, which is close to that of the respective celebrity. In the 6th column, the background is getting darker. In *handbag* \rightarrow *shoes* (Fig. 1a),

the color, texture and size of the shoes become closer to that of handbag. Additionally, for this experiment we plot the projections of the learned IT maps to the first 2 principal components of \mathbb{Q} (Fig. 11). We see that projections are close to \mathbb{Q} for $w = 1$ and become closer to \mathbb{P} with the increase of w . In *ffhq* \rightarrow *comics*, the changes mostly affect facial expressions and individual characteristics. In *textures* \rightarrow *chairs*, the changes are mostly related to chairs' size which is expected since we use pixel-wise ℓ^2 as the cost function. Additional qualitative results are given in Appendix F (Fig. 20, 21, 12).

For completeness, we measure test FID (Heusel et al., 2017) of the translated samples, see Table 2. We do not calculate FID in the *handbag* \rightarrow *chairs* experiment because of too small sizes of the test parts of the datasets (500 textures, 2K chairs). However, we emphasize that FID is not representative when $w > 1$. In this case, IT maps learn by construction only a part of the target measure \mathbb{Q} . At the same time, FID tests how well the transported samples represent the entire target distribution and is very sensitive to mode dropping (Lucic et al., 2018, Fig. 1b). Therefore, while the cost decreases with the growth of w , FID, on the contrary, increases. This is expected since IT maps to smaller part of \mathbb{Q} . Importantly, the visual quality of the translated images $\hat{T}(x)$ is not decreasing.

In Appendix C, we *compare* our IT method with CycleGAN and show that IT better preserves the input-output similarity.

¹kaggle.com/reitanaka/alignedanimefaces

²kaggle.com/datasets/defileroff/comic-faces-paired-synthetic-v2


 Figure 12: IT results for *textures* \rightarrow *chairs* (64×64).

Experiment	$w = 1$	$w = 2$	$w = 4$	$w = 8$
<i>celeba</i> \rightarrow <i>anime</i>	0.297	0.154	0.133	0.094
<i>handbag</i> \rightarrow <i>shoes</i>	0.368	0.320	0.259	0.252
<i>textures</i> \rightarrow <i>chairs</i>	0.603	0.516	0.474	0.408
<i>ffhq</i> \rightarrow <i>comics</i>	0.224	0.220	0.200	0.196

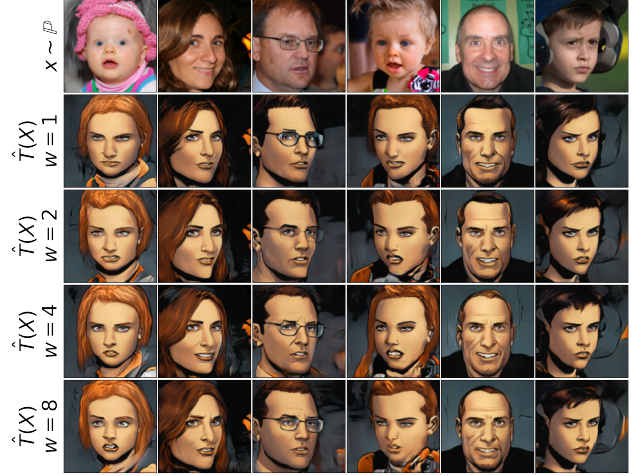
 Table 1: Test ℓ^2 transport cost of our learned IT maps.

6. Potential Impact

Inequality constraints for generative models. The majority of optimization objectives in generative models (GANs, diffusion models, normalizing flows, etc.) enforce the *equality* constraints, e.g., $T\#\mathbb{P} = \mathbb{Q}$, where $T\#\mathbb{P}$ is the generated measure and \mathbb{Q} is the data measure. Our work demonstrates that it is possible to enforce *inequality* constraints, e.g., $T\#\mathbb{P} \leq w\mathbb{Q}$, and apply them to a large-scale problem. While in this work we primarily focus on the image-to-image translation task, we believe that the ideas presented in our paper have several visible prospects for further improvement and applications. We list them below.

(1) Partial OT. Learning alignments between measures of *unequal* mass is a pervasive topic which has already perspective applications in biology to single-cell data (Yang & Uhler, 2018; Lübeck et al., 2022; Eyring et al., 2022). The mentioned works use unbalanced OT (Chizat, 2017). This is an unconstrained problem where the mass spread is softly controlled by the regularization. Therefore, may be hard to control how the mass is actually distributed. Using partial OT which enforces hard inequality constraints might potentially soften this issue. Our IT problem (12) is a particular case of partial OT (4). We believe that our study is useful for future development of partial OT methods.

(2) Generative nearest neighbors. NNs play an important role in machine learning applications such as, e.g., image retrieval (Babenko et al., 2014). These methods typically rely on fast *discrete* approximate NN (Malkov & Yashunin, 2018; Johnson et al., 2019) and perform *matching* with the latent codes of the train samples. In contrast, nowadays,


 Figure 13: IT results for *ffhq* \rightarrow *comics* (128×128).

Experiment	$w = 1$	$w = 2$	$w = 4$	$w = 8$
<i>celeba</i> \rightarrow <i>anime</i>	14.65	20.79	22.18	22.84
<i>handbag</i> \rightarrow <i>shoes</i>	27.10	29.70	42.90	53.80
<i>textures</i> \rightarrow <i>chairs</i>	N/A	N/A	N/A	N/A
<i>ffhq</i> \rightarrow <i>comics</i>	20.95	22.38	22.77	23.67

Table 2: Test FID of our learned IT maps.

with the rapid growth of large generative models such as DALL-E (Ramesh et al., 2022), CLIP (Radford et al., 2021), GPT-3 (Brown et al., 2020), it becomes relevant to perform *out-of-sample* estimation, e.g., map the latent vectors to *new* vectors which are not present in the train set to generate *new* data. Our IT approach (for $w \rightarrow \infty$) is a theoretically justified way to learn approximate NN maps exclusively from samples. We think our approach might acquire applications here as well, especially since there already exist ways to apply OT in latent spaces of such models (Fan et al., 2021).

(3) Robustness and outlier detection. Our IT aligns the input measure \mathbb{P} only with a part of the target measure \mathbb{Q} . This property might be potentially used to make the learning robust, e.g., ignore outliers in the target dataset. Importantly, the choice of outliers and contamination level are tunable via $c(x, y)$ and w , but their selection may be not obvious. At the same time, the potential f^* vanishes on the outliers, i.e., samples in $\text{Supp}(\mathbb{Q})$ to which the mass is not transported.

Proposition 4 (The potential vanishes at outliers). *Under the assumptions of Theorem 5, the equality $f^*(y) = 0$ holds for all $y \in \text{Supp}(\mathbb{Q}) \setminus \text{Supp}(T\#\mathbb{P})$.*

We empirically illustrate this statement in Appendix A. As a result of this proposition, a possible byproduct of our method is an outlier-score $f^*(y)$ for the target data. Such applications of OT are promising and there already exist works (Mukherjee et al., 2021; Balaji et al., 2020; Nietert et al., 2022) developing approaches to make OT more robust.

Limitations and societal impact. We discuss *limitations* of our study and its *societal impact* in Appendix A.

ACKNOWLEDGMENT. The work was supported by the Analytical center under the RF Government (subsidy agreement 000000D730321P5Q0002, Grant No. 70-2021-00145 02.11.2021).

References

- Aggarwal, D., Valiyev, E., Sener, F., and Yao, A. Learning style compatibility for furniture. In *German Conference on Pattern Recognition*, pp. 552–566. Springer, 2018.
- Aliprantis, C. D. and Border, K. C. Infinite dimensional analysis. Technical report, Springer, 2006.
- Alotaibi, A. Deep generative adversarial networks for image-to-image translation: A review. *Symmetry*, 12(10):1705, 2020.
- Arjovsky, M., Chintala, S., and Bottou, L. Wasserstein GAN. *arXiv preprint arXiv:1701.07875*, 2017.
- Asadulaev, A., Korotin, A., Egiazarian, V., and Burnaev, E. Neural optimal transport with general cost functionals. *arXiv preprint arXiv:2205.15403*, 2022.
- Babenko, A., Slesarev, A., Chigorin, A., and Lempitsky, V. Neural codes for image retrieval. In *European conference on computer vision*, pp. 584–599. Springer, 2014.
- Balaji, Y., Chellappa, R., and Feizi, S. Robust optimal transport with applications in generative modeling and domain adaptation. *Advances in Neural Information Processing Systems*, 33:12934–12944, 2020.
- Bińkowski, M., Sutherland, D. J., Arbel, M., and Gretton, A. Demystifying mmd gans. In *International Conference on Learning Representations*, 2018.
- Brown, T., Mann, B., Ryder, N., Subbiah, M., Kaplan, J. D., Dhariwal, P., Neelakantan, A., Shyam, P., Sastry, G., Askell, A., et al. Language models are few-shot learners. *Advances in neural information processing systems*, 33: 1877–1901, 2020.
- Caffarelli, L. A. and McCann, R. J. Free boundaries in optimal transport and monge-ampere obstacle problems. *Annals of mathematics*, pp. 673–730, 2010.
- Chen, H., He, X., Qing, L., Wu, Y., Ren, C., Sheriff, R. E., and Zhu, C. Real-world single image super-resolution: A brief review. *Information Fusion*, 79:124–145, 2022.
- Chen, X. and Jia, C. An overview of image-to-image translation using generative adversarial networks. In *International Conference on Pattern Recognition*, pp. 366–380. Springer, 2021.
- Chizat, L. *Unbalanced optimal transport: Models, numerical methods, applications*. PhD thesis, Université Paris sciences et lettres, 2017.
- Cimpoi, M., Maji, S., Kokkinos, I., Mohamed, S., , and Vedaldi, A. Describing textures in the wild. In *Proceedings of the IEEE Conf. on Computer Vision and Pattern Recognition (CVPR)*, 2014.
- Daniels, M., Maunu, T., and Hand, P. Score-based generative neural networks for large-scale optimal transport. *Advances in neural information processing systems*, 34: 12955–12965, 2021.
- de Bézenac, E., Ayed, I., and Gallinari, P. CycleGAN through the lens of (dynamical) optimal transport. In *Machine Learning and Knowledge Discovery in Databases. Research Track: European Conference, ECML PKDD 2021, Bilbao, Spain, September 13–17, 2021, Proceedings, Part II 21*, pp. 132–147. Springer, 2021.
- Eyring, L. V., Klein, D., Palla, G., Becker, S., Weiler, P., Kibertus, N., and Theis, F. Modeling single-cell dynamics using unbalanced parameterized monge maps. *bioRxiv*, 2022.
- Fan, J., Liu, S., Ma, S., Chen, Y., and Zhou, H. Scalable computation of monge maps with general costs. *arXiv preprint arXiv:2106.03812*, 2021.
- Figalli, A. The optimal partial transport problem. *Archive for rational mechanics and analysis*, 195(2):533–560, 2010.
- Folland, G. B. *Real analysis: modern techniques and their applications*, volume 40. John Wiley & Sons, 1999.
- Gazdieva, M., Rout, L., Korotin, A., Filippov, A., and Burnaev, E. Unpaired image super-resolution with optimal transport maps. *arXiv preprint arXiv:2202.01116*, 2022.
- Genevay, A., Cuturi, M., Peyré, G., and Bach, F. Stochastic optimization for large-scale optimal transport. In *Advances in neural information processing systems*, pp. 3440–3448, 2016.
- Genevay, A., Peyré, G., and Cuturi, M. Learning generative models with sinkhorn divergences. In *International Conference on Artificial Intelligence and Statistics*, pp. 1608–1617. PMLR, 2018.
- Goodfellow, I., Pouget-Abadie, J., Mirza, M., Xu, B., Warde-Farley, D., Ozair, S., Courville, A., and Bengio, Y. Generative adversarial nets. In *Advances in neural information processing systems*, pp. 2672–2680, 2014.
- Gulrajani, I., Ahmed, F., Arjovsky, M., Dumoulin, V., and Courville, A. C. Improved training of Wasserstein GANs.

- In *Advances in Neural Information Processing Systems*, pp. 5767–5777, 2017.
- Gushchin, N., Kolesov, A., Korotin, A., Vetrov, D., and Burnaev, E. Entropic neural optimal transport via diffusion processes. *arXiv preprint arXiv:2211.01156*, 2022.
- He, K., Zhang, X., Ren, S., and Sun, J. Deep residual learning for image recognition. In *Proceedings of the IEEE conference on computer vision and pattern recognition*, pp. 770–778, 2016.
- Henry-Labordere, P. (martingale) optimal transport and anomaly detection with neural networks: A primal-dual algorithm. *arXiv preprint arXiv:1904.04546*, 2019.
- Heusel, M., Ramsauer, H., Unterthiner, T., Nessler, B., and Hochreiter, S. GANs trained by a two time-scale update rule converge to a local nash equilibrium. In *Advances in neural information processing systems*, pp. 6626–6637, 2017.
- Huang, X., Liu, M.-Y., Belongie, S., and Kautz, J. Multi-modal unsupervised image-to-image translation. In *Proceedings of the European conference on computer vision (ECCV)*, pp. 172–189, 2018.
- Jing, Y., Yang, Y., Feng, Z., Ye, J., Yu, Y., and Song, M. Neural style transfer: A review. *IEEE transactions on visualization and computer graphics*, 26(11):3365–3385, 2019.
- Johnson, J., Douze, M., and Jégou, H. Billion-scale similarity search with gpus. *IEEE Transactions on Big Data*, 7(3):535–547, 2019.
- Karras, T., Laine, S., and Aila, T. A style-based generator architecture for generative adversarial networks. In *Proceedings of the IEEE/CVF conference on computer vision and pattern recognition*, pp. 4401–4410, 2019.
- Karush, W. Minima of functions of several variables with inequalities as side conditions. In *Traces and Emergence of Nonlinear Programming*, pp. 217–245. Springer, 2014.
- Kingma, D. P. and Ba, J. Adam: A method for stochastic optimization. *arXiv preprint arXiv:1412.6980*, 2014.
- Korotin, A., Egiastian, V., Asadulaev, A., Safin, A., and Burnaev, E. Wasserstein-2 generative networks. In *International Conference on Learning Representations*, 2021a. URL https://openreview.net/forum?id=bEoxzW_EXsa.
- Korotin, A., Li, L., Genevay, A., Solomon, J., Filippov, A., and Burnaev, E. Do neural optimal transport solvers work? a continuous wasserstein-2 benchmark. *arXiv preprint arXiv:2106.01954*, 2021b.
- Korotin, A., Kolesov, A., and Burnaev, E. Kantorovich strikes back! wasserstein gans are not optimal transport? In *Thirty-sixth Conference on Neural Information Processing Systems Datasets and Benchmarks Track*, 2022a.
- Korotin, A., Selikhanovych, D., and Burnaev, E. Kernel neural optimal transport. *arXiv preprint arXiv:2205.15269*, 2022b.
- Korotin, A., Selikhanovych, D., and Burnaev, E. Neural optimal transport. *arXiv preprint arXiv:2201.12220*, 2022c.
- Liu, H., Gu, X., and Samaras, D. Wasserstein GAN with quadratic transport cost. In *Proceedings of the IEEE International Conference on Computer Vision*, pp. 4832–4841, 2019.
- Liu, Z., Luo, P., Wang, X., and Tang, X. Deep learning face attributes in the wild. In *Proceedings of International Conference on Computer Vision (ICCV)*, December 2015.
- Lübeck, F., Bunne, C., Gut, G., del Castillo, J. S., Pelkmans, L., and Alvarez-Melis, D. Neural unbalanced optimal transport via cycle-consistent semi-couplings. *arXiv preprint arXiv:2209.15621*, 2022.
- Lucic, M., Kurach, K., Michalski, M., Gelly, S., and Bousquet, O. Are GANs created equal? a large-scale study. In *Advances in neural information processing systems*, pp. 700–709, 2018.
- Makkuva, A. V., Taghvaei, A., Oh, S., and Lee, J. D. Optimal transport mapping via input convex neural networks. *arXiv preprint arXiv:1908.10962*, 2019.
- Malkov, Y. A. and Yashunin, D. A. Efficient and robust approximate nearest neighbor search using hierarchical navigable small world graphs. *IEEE transactions on pattern analysis and machine intelligence*, 42(4):824–836, 2018.
- Mathur, A., Isopoussu, A., Kawsar, F., Berthouze, N., and Lane, N. D. Mic2mic: using cycle-consistent generative adversarial networks to overcome microphone variability in speech systems. In *Proceedings of the 18th international conference on information processing in sensor networks*, pp. 169–180, 2019.
- Mukherjee, D., Guha, A., Solomon, J. M., Sun, Y., and Yurochkin, M. Outlier-robust optimal transport. In *International Conference on Machine Learning*, pp. 7850–7860. PMLR, 2021.
- Nhan Dam, Q. H., Le, T., Nguyen, T. D., Bui, H., and Phung, D. Threeplayer Wasserstein GAN via amortised duality. In *Proc. of the 28th Int. Joint Conf. on Artificial Intelligence (IJCAI)*, 2019.

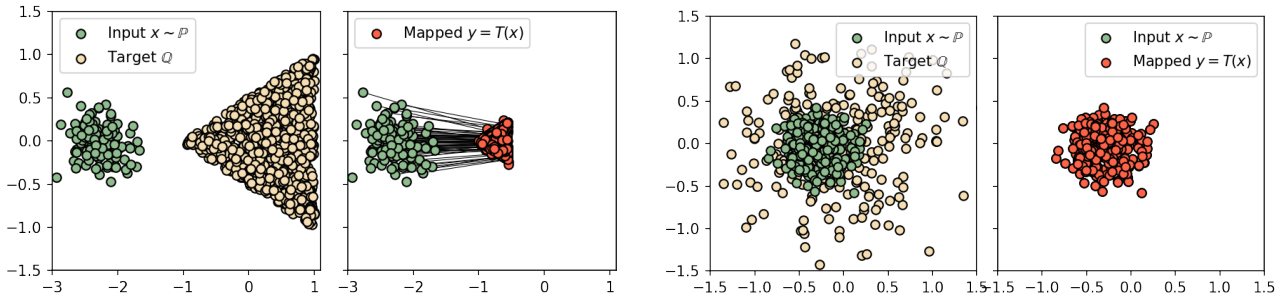
- Nietert, S., Goldfeld, Z., and Cummings, R. Outlier-robust optimal transport: Duality, structure, and statistical analysis. In *International Conference on Artificial Intelligence and Statistics*, pp. 11691–11719. PMLR, 2022.
- Pang, Y., Lin, J., Qin, T., and Chen, Z. Image-to-image translation: Methods and applications. *IEEE Transactions on Multimedia*, 2021.
- Peyré, G., Cuturi, M., et al. Computational optimal transport. *Foundations and Trends® in Machine Learning*, 11(5-6): 355–607, 2019.
- Radford, A., Kim, J. W., Hallacy, C., Ramesh, A., Goh, G., Agarwal, S., Sastry, G., Askell, A., Mishkin, P., Clark, J., et al. Learning transferable visual models from natural language supervision. In *International Conference on Machine Learning*, pp. 8748–8763. PMLR, 2021.
- Ramesh, A., Dhariwal, P., Nichol, A., Chu, C., and Chen, M. Hierarchical text-conditional image generation with clip latents. *arXiv preprint arXiv:2204.06125*, 2022.
- Rockafellar, R. T. Integral functionals, normal integrands and measurable selections. In *Nonlinear operators and the calculus of variations*, pp. 157–207. Springer, 1976.
- Ronneberger, O., Fischer, P., and Brox, T. U-net: Convolutional networks for biomedical image segmentation. In *International Conference on Medical image computing and computer-assisted intervention*, pp. 234–241. Springer, 2015.
- Rout, L., Korotin, A., and Burnaev, E. Generative modeling with optimal transport maps. *arXiv preprint arXiv:2110.02999*, 2021.
- Santambrogio, F. Optimal transport for applied mathematicians. *Birkhäuser, NY*, 55(58-63):94, 2015.
- Seguy, V., Damodaran, B. B., Flamary, R., Courty, N., Rolet, A., and Blondel, M. Large-scale optimal transport and mapping estimation. *arXiv preprint arXiv:1711.02283*, 2017.
- Terkelsen, F. Some minimax theorems. *Mathematica Scandinavica*, 31(2):405–413, 1972.
- Villani, C. *Optimal transport: old and new*, volume 338. Springer Science & Business Media, 2008.
- Yang, K. D. and Uhler, C. Scalable unbalanced optimal transport using generative adversarial networks. In *International Conference on Learning Representations*, 2018.
- Yu, A. and Grauman, K. Fine-grained visual comparisons with local learning. In *Proceedings of the IEEE Conference on Computer Vision and Pattern Recognition*, pp. 192–199, 2014.
- Yu, F., Seff, A., Zhang, Y., Song, S., Funkhouser, T., and Xiao, J. Lsun: Construction of a large-scale image dataset using deep learning with humans in the loop. *arXiv preprint arXiv:1506.03365*, 2015.
- Yuan, Y., Liu, S., Zhang, J., bing Zhang, Y., Dong, C., and Lin, L. Unsupervised image super-resolution using cycle-in-cycle generative adversarial networks. *2018 IEEE/CVF Conference on Computer Vision and Pattern Recognition Workshops (CVPRW)*, pp. 814–81409, 2018.
- Zhang, R., Isola, P., Efros, A. A., Shechtman, E., and Wang, O. The unreasonable effectiveness of deep features as a perceptual metric. In *CVPR*, 2018.
- Zhang, X., Zhai, D., Li, T., Zhou, Y., and Lin, Y. Image inpainting based on deep learning: A review. *Information Fusion*, 2022.
- Zhu, J.-Y., Park, T., Isola, P., and Efros, A. A. Unpaired image-to-image translation using cycle-consistent adversarial networks. In *Proceedings of the IEEE international conference on computer vision*, pp. 2223–2232, 2017.

A. Limitations

Transport costs. Our theoretical results hold true for any continuous cost function $c(x, y)$, but our experimental study uses ℓ^2 as it already yields a reasonable performance in many cases. Considering more semantically meaningful costs for image translation, e.g., perceptual (Zhang et al., 2018), is a promising future research direction.

Intersecting supports. ET is the nearest neighbor assignment (§3.1). Using ET may be unreasonable when $\mathcal{X} = \mathcal{Y}$ and $\text{Supp}(\mathbb{P})$ intersects with $\text{Supp}(\mathbb{Q})$. For example, if $c(x, y)$ attains minimum over $y \in \mathcal{Y}$ for a given $x \in \mathcal{X}$ at $x = y$, e.g., $c = \ell^2$, then there exists a ET plan satisfying $\pi^*(y|x) = \delta_x$ for all $x \in \text{Supp}(\mathbb{P}) \cap \text{Supp}(\mathbb{Q})$. It does not move the mass of points x in this intersection. We provide an illustrative toy 2D example in Fig. 14b.

Limited diversity. It is theoretically impossible to preserve input-output similarity better than ET maps. Still one should understand that in some cases these maps may yield degenerate solutions. In Fig. 14a, we provide a toy 2D example of an IT map ($w = 8$) which maps all inputs to nearly the same point. In Fig. 12 (*texture* \rightarrow *chair* translation), we see that with the increase of w the IT map produces less small chairs but more large armchairs. In particular, when $w = 8$, only armchairs appear, see Fig. 12. This is because they are closer (in ℓ^2) to textures due to having smaller white background area.



(a) **Limited diversity.** The true ET map is degenerate: it maps the entire \mathbb{P} to a single vertex of the triangle \mathbb{Q} . The example shows the learned IT map with high $w = 20$ approximating the ET map.

(b) **Intersecting supports.** The true ET map is the identity map: it does not move the probability mass of \mathbb{P} . The example shows the learned IT map with high $w = 8$ approximating the ET map.

Figure 14: Toy 2D examples showing two (potential) limitations of IT maps.

Unused samples. Doing experiments, we noticed that the model training slows down with the increase of w . A possible cause of this is that some samples from \mathbb{Q} become non-informative for training (this follows from our Proposition 4). Intuitively, the part of $\text{Supp}(\mathbb{Q})$ to which the samples of \mathbb{P} will *not* be mapped to is not informative for training. We illustrate this effect on toy 'Wi-Fi' example and plot the histogram of values of f^* in Fig. 15. One possible negative of this observation is that the training of IT maps or, more generally, partial OT maps, may naturally require larger training datasets.

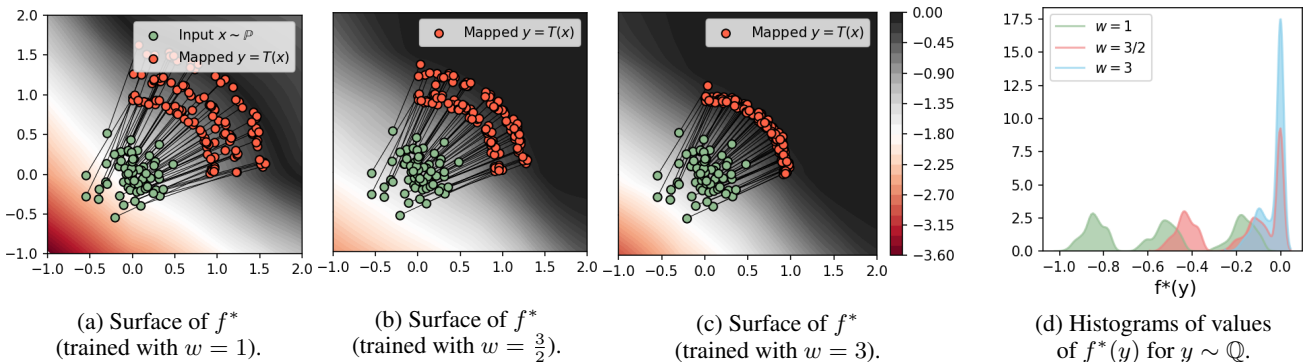


Figure 15: Illustration the **unused samples**. In Figures 15a, 15b, 15c, we visualize the surface of the learned potential f^* on the 'Wi-Fi' example and $w \in \{1, \frac{3}{2}, 3\}$. In Figures 15b, 15c, the potential vanishes on the arcs of \mathbb{Q} to which the mass of \mathbb{P} is not mapped, i.e., $f^*(y) = 0$. In Figure 15d, we plot the distribution of values of $f^*(y)$ for $y \sim \mathbb{Q}$. For $w \in \{\frac{3}{2}, 3\}$, we see large pikes around $f^*(y) = 0$ further demonstrating that the potential equals to zero on a certain part of \mathbb{Q} .

Limited quantitative metrics. In experiments (§5), we use a limited amount of quantitative metrics. This is because existing unpaired metrics, e.g., FID (Heusel et al., 2017), KID (Bińkowski et al., 2018), etc., are **not suitable for our setup**.

They aim to test equalities, such as $T\#\mathbb{P} = \mathbb{Q}$, while our learned maps disobey it *by the construction* (they capture only a part of \mathbb{Q}). Developing quality metrics for *partial* generative models is an important future research direction. Meanwhile, for our method, we have provided a toy 2D analysis (§5.1) and explanatory metrics (§5.2), such as the transport cost (Table 1).

Inexistent IT maps. The actual IT plans between \mathbb{P}, \mathbb{Q} may be non-deterministic, while our approach only learns a deterministic map T . Nevertheless, thanks to our Proposition 3, for every $\epsilon > 0$ there always exists a 1-to-1 map $T_\epsilon\#\mathbb{P} \leq w\mathbb{Q}$ which provides ϵ -sub-optimal cost $\int_{\mathcal{X}} c(x, T_\epsilon(x)) d\mathbb{P}(x) \leq \text{Cost}_w(\mathbb{P}, \mathbb{Q}) + \epsilon$. Thus, IT cost (12) can be approached arbitrary well with deterministic transport maps. A potential way to modify our algorithm is to learn stochastic plans is to add random noise z to generator $T(x, z)$ as input, although this approach may suffer from ignoring z , see (Korotin et al., 2022c, §5.1).

Fake solutions and instabilities. Lagrangian objectives such as (15) may potentially have optimal saddle points (f^*, T^*) in which T^* is not an OT map. Such T^* are called *fake solutions* (Korotin et al., 2022b) and may be one of the causes of training instabilities. Fake solutions can be removed by considering OT with strictly convex *weak* costs functions (Korotin et al., 2022c, Appendix H). In the context of partial OT, we leave this question open for future work.

Potential societal impact. Neural OT methods and, more generally, generative models are a developing research direction. They find applications such as style translation and realistic content generation. We expect that our method may improve existing applications of generative models and add new directions of neural OT usage like outlier detection. However, it should be taken into account that generative models can also be used for negative purposes such as creating fake faces.

B. Toy 2D Illustrations of Other Methods

In this section, we demonstrate how the other methods perform in ‘Wi-Fi’ and ‘Accept’ experiments. We start with ‘Wi-Fi’. Assume that we would like to map \mathbb{P} to the closest $\frac{2}{3}$ -rd fraction of \mathbb{Q} , i.e., we aim to learn 2 of 3 arcs in \mathbb{Q} , (as in Fig. 10c).

In Fig. 16d, we show the discrete partial OT (4) with parameters $w_0 = m = 1$ and $w_1 = \frac{3}{2}$, which correspond to IT (12) with $w = \frac{3}{2}$. To obtain the discrete matching, we run `ot.partial.partial.wasserstein2` from POT³. As expected, it matches the input \mathbb{P} with $\frac{2}{3}$ of \mathbb{Q} and can be viewed as the ground truth (coinciding with our Fig. 10c).

First, we show the GAN (Goodfellow et al., 2014) endowed with additional ℓ^2 loss with weight $\lambda = 0.5$ (in Fig. 16a). Next, we consider discrete unbalanced OT (Chizat, 2017) with the quadratic cost $c = \ell^2$. In Fig. 16b, we show the results of the matching obtained by `ot.unbalanced` with parameters $m = 1, \text{reg} = 0.1, \text{reg}_m = 1, \text{numItermax} = 200000$. Additionally, in Fig. 16c we show the result of neural unbalanced OT method (Yang & Uhler, 2018).⁴ To make their unbalanced setup maximally similar to our IT, we set to zero their regularization parameters. The rest parameters are default except for $\lambda_0 = 0.02$ (ℓ^2 loss parameter), $\lambda_2 = 5$ (input and target measures’ variation parameter).

We see that GAN+ ℓ^2 (Fig. 16a) and unbalanced OT (Fig. 16b and 16c) indeed match \mathbb{P} with only a *part* of the target measure \mathbb{Q} . The transported mass is mostly concentrated in the two small arcs of \mathbb{Q} which are closest to \mathbb{P} w.r.t. ℓ^2 cost. The issue here is that some mass of \mathbb{P} spreads over the third (biggest) arc of \mathbb{Q} yielding **outliers**. This happens because unbalanced OT (GAN can be viewed as its particular case) is an *unconstrained* problem: the mass spreading is controlled via soft penalization (f -divergence loss term). The lack of hard constraints, such as those in partial OT (4) or IT (12), makes it challenging to strictly control how the mass in unbalanced OT actually spreads.

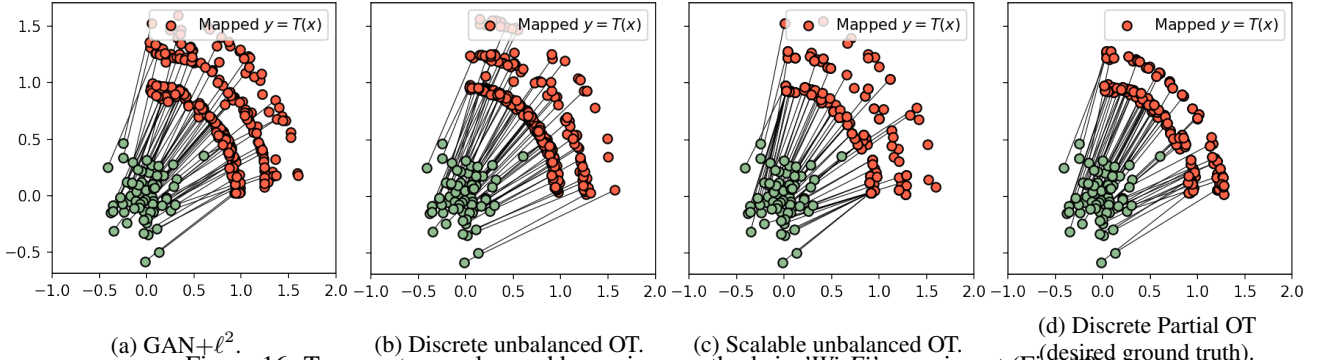


Figure 16: Transport maps learned by various methods in ‘Wi-Fi’ experiment (Fig. 10a).

For completeness, we also show the results of these methods applied to ‘Accept’ experiment, see Fig. 17. Here we tested

³pythonot.github.io

⁴github.com/uhlerlab/unbalanced_ot

various hyperparameters for these methods but did not achieve the desired behaviour, i.e., learning only the text ‘Accept’. Moreover, we noted that $\text{GAN} + \ell^2$ for large λ yields undesirable artifacts (Fig. 17a). This is because GAN and ℓ^2 losses contradict to each other and still the models tried to minimize them both. We further discuss in Appendix C below.

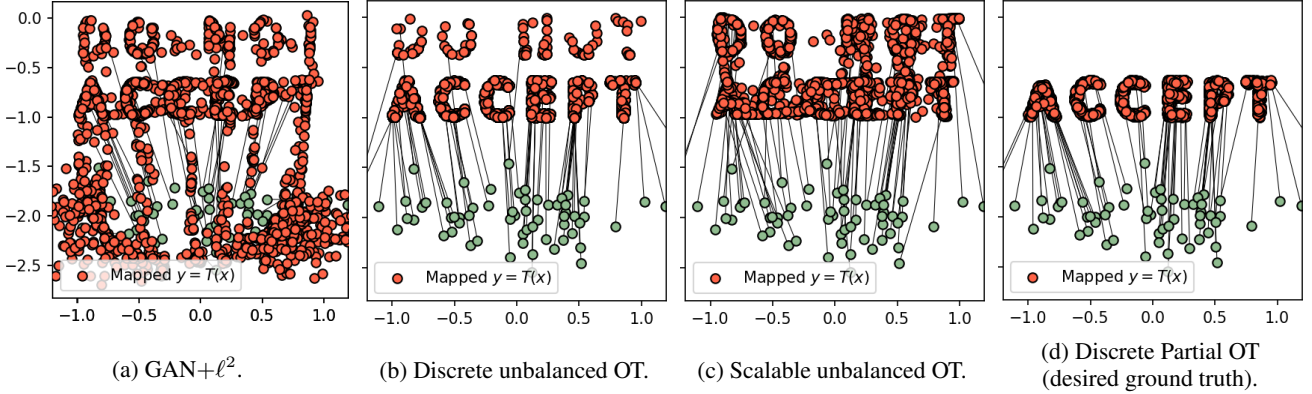


Figure 17: Transport maps learned by various methods in ‘Accept’ experiment.

C. Comparison with CycleGANs

Recall that ET by design is the best translation between a pair of domains w.r.t. the **given** dissimilarity function $c(x, y)$. Our IT maps with the increase of w provide better input-output similarity and recover ET when $w \rightarrow \infty$ (§3.3). A reader may naturally ask: **(a)** How else can we recover ET maps? **(b)** To which extent one can control the input-output similarity in existing translation methods? **(c)** Can these methods be used to approximate ET? We discuss these aspects below.

Many translation methods are based on GANs, see (Pang et al., 2021; Alotaibi, 2020; Chen & Jia, 2021) for a survey. Their learning objectives are usually combined of several loss terms:

$$\mathcal{L}_{\text{Total}}(T) \stackrel{\text{def}}{=} \mathcal{L}_{\text{Dom}}(T) + \lambda \cdot \mathcal{L}_{\text{Sim}}(T) + [\text{other terms}]. \quad (17)$$

In (17), the **domain loss** \mathcal{L}_{Dom} is usually the vanilla GAN loss involving a discriminator (Goodfellow et al., 2014) ensuring that the learned map $x \mapsto T(x)$ transforms inputs $x \sim \mathbb{P}$ to the samples from the target data distribution \mathbb{Q} . The **similarity loss** \mathcal{L}_{Sim} (with $\lambda \geq 0$) is usually the *identity* loss $\int_{\mathcal{X}} \|x - T(x)\|_1 d\mathbb{P}(x)$. More generally, it can be an arbitrary *unsupervised* loss of the form $\int_{\mathcal{X}} c(x, T(x)) d\mathbb{P}(x)$ stimulating the output sample $T(x)$ to look like the input samples x w.r.t. given dissimilarity function c , e.g., ℓ^1 , ℓ^2 , ℓ^p , perceptual, etc. The other terms in (17) involve model-specific terms (e.g., cycle consistency loss in CycleGAN) which are not related to our study.

When learning a model via optimizing (17), a natural way to get better similarity of x and $T(x)$ in (17) is to simply increase weight λ of the corresponding loss term. This is a straightforward approach but it has a visible **limitation**. When λ is high, the term $\lambda \cdot \mathcal{L}_{\text{Sim}}$ dominates over the other terms such as \mathcal{L}_{Dom} , and the model T simply learns to minimize this loss ignoring the fact that the output sample should be from the target data distribution \mathbb{Q} . In other words, in (17) there is a nasty **trade-off** between $T(x)$ belonging to the target data distribution \mathbb{Q} and input-output similarity of x and $T(x)$. The parameter $\lambda \geq 0$ controls this *realism-similarity* trade-off, and we study how it affects the learned map T below.

We pick **CycleGAN** (Zhu et al., 2017) as a model for evaluation. The method has $> 15\text{k}$ citations (according to Google Scholar), which makes CycleGAN one of the principal models to solve the unpaired translation problem. We train the model on *celeba* \rightarrow *anime* (64×64) and *handbags* \rightarrow *shoes* (128×128) translation with various λ and report the qualitative and quantitative results below. An the similarity loss, we use $c = \ell^1$ as the authors **originally used in their paper**.⁵

Results and discussion. In all cases, we report both ℓ^2 and ℓ^1 transport costs and FID on the test samples. Tables 3 and 4 shows transport costs and FID of CycleGAN. FID and ℓ^2 metrics for our method are given in the main text (Tables 2, 1) and ℓ^1 cost is given in Table 5 below. For convenience, we visualize (FID, Cost) pairs for our method and CycleGAN in Fig. 18.

⁵We also conducted a separate experiment to train CycleGAN with ℓ^2 identity loss. However, in this case CycleGAN’s training turned to be less stable and, importantly, yielded (mostly) worse FID. Surprisingly, we observed higher test transport costs (both ℓ^2 and ℓ^1). Therefore, not to overload the exposition, we decided to keep only the experiment with CycleGAN trained with ℓ^1 identity loss.

Interestingly, we see that adding small identity loss $\lambda = 50$ yields not only decrease of the transport cost (compared to $\lambda = 0$), but some improvement of FID as well. Still we see that the transport cost in CycleGAN naturally decreases with the increase of weight λ after $\lambda \approx 50$ -100. Unfortunately, this decrease is accompanied by the **decrease** of the visual image quality, see Fig. 19. While for large λ the cost is really small, these CycleGAN models are **practically useless** because they poor image quality. In particular, for very large λ , CycleGAN simply learns the identity map, as expected.

For λ providing acceptable visual quality, CycleGAN yields a transport cost which is bigger than that of standard OT ($w = 1$). Our IT with $w = 2$ easily yields smaller transport cost (better similarity), and the result for $w = 8$ is unachievable for CycleGAN. Note that in most cases FID is smaller than that of CycleGAN.

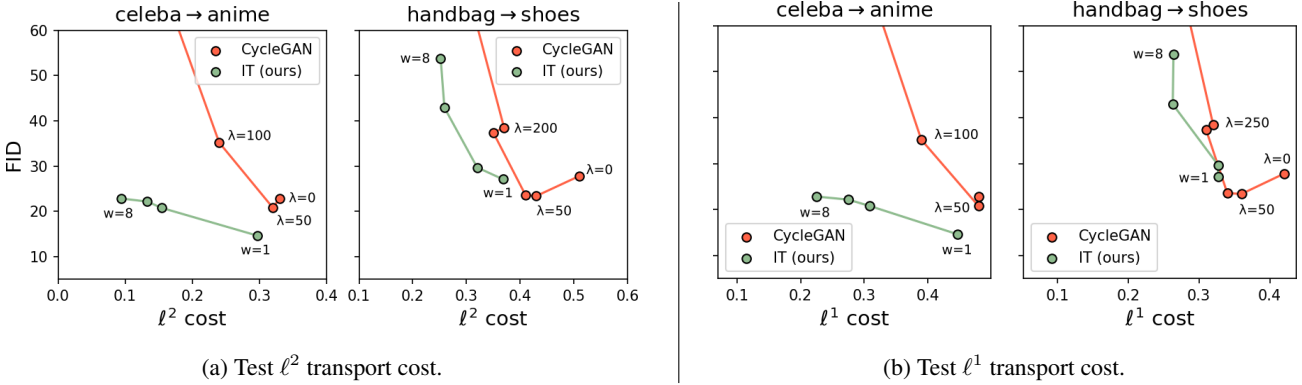
Experiment	Cost	$\lambda = 0$	$\lambda = 50$	$\lambda = 100$	$\lambda = 200$	$\lambda = 250$	$\lambda = 300$	$\lambda = 350$	$\lambda = 500$
<i>celeba</i> \rightarrow <i>anime</i>	ℓ^1	0.48	0.48	0.39	0.26	0.09	0.09	0.09	0.09
<i>handbag</i> \rightarrow <i>shoes</i>		0.42	0.36	0.34	0.31	0.32	0.22	0.16	0.07
<i>celeba</i> \rightarrow <i>anime</i>	ℓ^2	0.33	0.32	0.24	0.11	0.01	0.02	0.02	0.01
<i>handbag</i> \rightarrow <i>shoes</i>		0.51	0.43	0.41	0.35	0.37	0.22	0.14	0.02

 Table 3: Test ℓ^1 and ℓ^2 transport cost of CycleGAN.

Experiment	$\lambda = 0$	$\lambda = 50$	$\lambda = 100$	$\lambda = 200$	$\lambda = 250$	$\lambda = 300$	$\lambda = 350$	$\lambda = 500$
<i>celeba</i> \rightarrow <i>anime</i>	22.9	20.8	35.2	88.8	122.2	123.5	120.0	122.8
<i>handbag</i> \rightarrow <i>shoes</i>	27.8	23.4	23.6	37.4	38.5	105.6	144.9	152.9

Table 4: Test FID of CycleGAN.

Experiment	$w = 1$	$w = 2$	$w = 4$	$w = 8$
<i>celeba</i> \rightarrow <i>anime</i>	0.447	0.309	0.275	0.225
<i>handbag</i> \rightarrow <i>shoes</i>	0.327	0.328	0.263	0.264

 Table 5: Test ℓ^1 transport cost of our IT maps (learned with ℓ^2 transport cost).

 Figure 18: Comparison of test FID and transport costs (ℓ^2 and ℓ^1) of our IT method and CycleGAN.

Concluding remarks. Our algorithm with $w \rightarrow \infty$ allows us to achieve better similarity without the decrease of the image quality. At the same time, CycleGAN fails to do this when $\lambda \rightarrow \infty$. Why does this happen?

We again emphasize that typical GAN objective (17) consists of several loss terms. Each term stimulates the model to attain certain properties (realism, similarity to the input, etc.). These terms, in general, *contradict* each other as they have different minima T . This yields the nasty **trade-off** between the loss terms.

In contrast, **our method is not a sum of losses**. Our objective (15) may look like a direct sum of a transport cost with an adversarial loss; our method does have a generator (transport maps T) and a discriminator (potential f) which are trained via the saddle-point optimization objective $\max_f \min_T$. Yet, this visible **similarity to GAN-based methods is deceptive**. Our objective $\max_f \min_T$ can be viewed as a Lagrangian and is **atypical** for GANs: the generator is in the inner optimization problem \min_T while in GANs the objective is $\min_T \max_f$. In our case, similar to other neural dual OT methods, the generator is adversarial to the discriminator but not vice versa, as in GANs. Please consult (Korotin et al., 2022c, §4.3), (Gazdieva et al., 2022, §6.2) or (Fan et al., 2021, §3) for further discussion about OT methods.

GANs aim to balance loss terms \mathcal{L}_{Dom} and \mathcal{L}_{Sim} . Our optimization objective enforces the constraint $T\#P \leq wQ$ via learning the potential f (a.k.a. Lagrange multiplier) and among admissible maps T searches for the one providing the smallest transport cost. There is no realism-similarity trade-off. For completeness, we emphasize that when $w \rightarrow \infty$, FID in Table 2 does not drop because of the decrease of the image quality, but because our method covers the less part of Q . FID negatively reacts to this (Lucic et al., 2018, Fig. 1b).



(a) *Celeba (female) \rightarrow anime* (64×64).

(b) *Handbags \rightarrow shoes* (128×128).

Figure 19: Unpaired translation with CycleGAN endowed with ℓ^1 identity loss with various weights λ .

D. Experimental Details

Pre-processing. For all datasets, we rescale images’ RGB channels to $[-1, 1]$. As in (Korotin et al., 2021b), we rescale aligned anime face images to 512×512 . Then we do 256×256 crop with the center located 14 pixels above the image center to get the face. Finally, for all datasets except the textures dataset, we resize the images to the required size (64×64 or 128×128). We apply random horizontal flipping augmentation to the comic faces and chairs datasets. Analogously to (Korotin et al., 2022b), we rescale describable textures to minimal border size of 300, do the random resized crop (from 128 to 300 pixels) and random horizontal and vertical flips. Next, we resize images to the required size (64×64 or 128×128).

Neural networks. In §5.1, we use fully connected networks both for the mapping T_θ and potential f_ψ . In §5.2, we use UNet (Ronneberger et al., 2015) architecture for the transport map T_θ . We use WGAN-QC’s (Liu et al., 2019) ResNet (He et al., 2016) discriminator as a potential f_ψ . We add an additional final layer $x \mapsto -|x|$ to f_ψ to make its outputs non-positive.

Optimization. We employ Adam (Kingma & Ba, 2014) optimizer with the default betas both for T_θ and f_ψ . The learning rate is $lr = 10^{-4}$. We use the MultiStepLR scheduler which decreases lr by 2 after $[(5+5 \cdot w)K, (20+5 \cdot w)K, (40+5 \cdot w)K, (70+5 \cdot w)K]$ iterations of f_ψ where $w \in \{1, 2, 4, 8\}$ is a weight parameter. The batch size is $|X| = 256$ for toy ‘Wi-Fi’, $|X| = 4096$ for toy Accept, and $|X| = 64$ for image-to-image translation experiments. The number of inner T_θ iterations is $k_T = 10$. In toy experiments, we observe convergence in $\approx 30K$ total iterations of f_ψ for ‘Wi-Fi’, in $\approx 70K$ for Accept. In the image-to-image translation, we do $\approx 70K$ iterations for 128×128 datasets, $\approx 40K$ iterations for 64×64 datasets. In the experiments with image-to-image translation experiments, we gradually increase w for 20K first iterations of f_ψ . We start from $w = 1$ and linearly increase it to the desired w (2, 4 or 8).

Computational complexity. The complexity of training IT maps depends on the dataset, size of images and weight w . Convergence time increases with the increase of w : possible reasons for this are discussed in the *unused samples* limitation (Appendix A). In general, it takes from 2 (for $w = 1$) up to 6 (for $w = 8$) days on a single Tesla V100 GPU.

Reproducibility. We provide the code for the experiments and will provide the trained models, see `README.md`.

E. Proofs

Proof of Proposition 1. Since continuous c is defined on a compact set $\mathcal{X} \times \mathcal{Y}$, it is uniformly continuous on $\mathcal{X} \times \mathcal{Y}$. This means that there exists a modulus of continuity $\omega : [0, +\infty) \rightarrow [0, \infty)$ such that for all $(x, y), (x', y') \in \mathcal{X} \times \mathcal{Y}$ it holds

$$|c(x, y) - c(x', y')| \leq \omega(\|x - x'\|_{\mathcal{X}} + \|y - y'\|_{\mathcal{Y}}),$$

and function ω is monotone, continuous at 0 with $\omega(0) = 0$. In particular, for $y = y'$ we have $|c(x, y) - c(x', y)| \leq \omega(\|x - x'\|_{\mathcal{X}})$. Thus, for $c^*(x) = \min_{y \in \text{Supp}(\mathbb{Q})} c(x, y)$, we have $|c^*(x) - c^*(x')| \leq \omega(\|x - x'\|_{\mathcal{X}})$, see (Santambrogio, 2015, Box 1.8). This means that $c^* : \mathcal{X} \rightarrow \mathbb{R}$ is (uniformly) continuous. \square

Proof of Theorem 1. Since function $(x, y) \mapsto c(x, y)$ is continuous, there exists a measurable selection $T^* : \mathcal{X} \rightarrow \mathcal{Y}$ from the set-valued map $x \mapsto \arg \min_{y \in \text{Supp}(\mathbb{Q})} c(x, y)$, see (Aliprantis & Border, 2006, Theorem 18.19). This map for all $x \in \mathcal{X}$ satisfies $c(x, T(x)) = \min_{y \in \text{Supp}(\mathbb{Q})} c(x, y) = c^*(x)$. As a result, $\int_{\mathcal{X}} c(x, T(x)) d\mathbb{P}(x) = \int_{\mathcal{X}} c^*(x) d\mathbb{P}(x)$ and (7) is tight. \square

Lemma 1. (Distinctness) Let $\mu, \nu \in \mathcal{M}(\mathcal{Y})$. Then $\mu \leq \nu$ holds if and only if for every $f \in \mathcal{C}(\mathcal{Y})$ satisfying $f \leq 0$ it holds that $\int_{\mathcal{Y}} f(y) d\mu(y) \geq \int_{\mathcal{Y}} f(y) d\nu(y)$.

Proof of Lemma 1. If $\mu \leq \nu$, then the inequality $\int_{\mathcal{Y}} f(y) d(\mu - \nu)(y) \geq 0$ for every (measurable) $f \leq 0$ follows from the definition of the Lebesgue integral. Below we prove the statement in the other direction.

Assume the opposite, i.e., $\int_{\mathcal{Y}} f(y) d(\mu - \nu)(y) \geq 0$ for every continuous $f \leq 0$ but still $\nu \not\leq \mu$. The latter means there exists a measurable $A \subset \mathcal{Y}$ satisfying $\mu(A) > \nu(A)$. Let $\epsilon = \frac{1}{2}(\mu(A) - \nu(A)) > 0$. Consider the negative indicator function $f_A(y)$ which equals -1 if $y \in A$ and 0 when $y \notin A$. Consider a variation measure $|\nu - \mu| \in \mathcal{M}_+(\mathcal{Y})$. Thanks to (Folland, 1999, Proposition 7.9), the continuous functions $\mathcal{C}(\mathcal{Y})$ are dense in the space $\mathcal{L}^1(|\mu - \nu|)$. Therefore, there exists a function $f_{A,\epsilon} \in \mathcal{C}(\mathcal{Y})$ satisfying $\int_{\mathcal{X}} |f_A(y) - f_{A,\epsilon}(y)| d|\mu - \nu|(y) < \epsilon$. We define $f_{A,\epsilon}^-(y) \stackrel{\text{def}}{=} \min\{0, f_{A,\epsilon}(y)\} \leq 0$. This is a non-positive continuous function, and for $y \in \mathcal{Y}$ it holds that $|f_A(y) - f_{A,\epsilon}(y)| \geq |f_A(y) - f_{A,\epsilon}^-(y)|$ because $f_{A,\epsilon}$ takes only non-positive values $\{0, -1\}$. We derive

$$\begin{aligned} \int_{\mathcal{Y}} f_{A,\epsilon}^-(y) d(\mu - \nu)(y) &= \overbrace{\int_{\mathcal{Y}} f_A(y) d(\mu - \nu)(y)}^{=\nu(A) - \mu(A) = -2\epsilon} + \int_{\mathcal{Y}} (f_{A,\epsilon}^-(y) - f_A(y)) d(\mu - \nu)(y) \leq \\ &-2\epsilon + \int_{\mathcal{Y}} |f_{A,\epsilon}^-(y) - f_A(y)| d|\mu - \nu|(y) \leq -2\epsilon + \int_{\mathcal{Y}} |f_{A,\epsilon}(y) - f_A(y)| d|\mu - \nu|(y) \leq -2\epsilon + \epsilon = -\epsilon < 0, \end{aligned}$$

which is a contradiction to the fact that $\int_{\mathcal{Y}} f(y) d(\mu - \nu)(y) \geq 0$ for every continuous $f \leq 0$. Thus, $\mu \leq \nu$. \square

Proof of Proposition 3. Let $\pi^* \in \Pi^w(\mathbb{P}, \mathbb{Q})$ be an IT plan. Consider the OT problem between \mathbb{P} and π_y^* :

$$\min_{\pi \in \Pi(\mathbb{P}, \pi_y^*)} \int_{\mathcal{X} \times \mathcal{Y}} c(x, y) d\pi(x, y). \quad (18)$$

It turns out that π^* is a minimizer here. Assume the contrary, i.e., that there exists a more optimal $\pi' \in \Pi(\mathbb{P}, \pi_y^*)$ satisfying

$$\int_{\mathcal{X} \times \mathcal{Y}} c(x, y) d\pi'(x, y) < \int_{\mathcal{X} \times \mathcal{Y}} c(x, y) d\pi^*(x, y) \quad (= \text{Cost}_w(\mathbb{P}, \mathbb{Q})). \quad (19)$$

This plan by the definition of $\Pi(\mathbb{P}, \pi_y^*)$ satisfies $\pi'_x = \mathbb{P}$ and $\pi'_y = \pi_y^* \leq w\mathbb{Q}$, i.e., $\pi' \in \Pi^w(\mathbb{P}, \mathbb{Q})$. However, (19) contradicts the fact that π^* is an IT plan in (18) as π' provides smaller cost. Thus, min in (18) equals $\text{Cost}_w(\mathbb{P}, \mathbb{Q})$ in (12).

Thanks to (Santambrogio, 2015, Theorem 1.33), problem (18) has the same minimal value as the inf in the Monge's problem

$$\inf_{T \# \mathbb{P} = \pi_y^*} \int_{\mathcal{X}} c(x, T(x)) d\mathbb{P}(x), \quad (20)$$

i.e., for every $\epsilon > 0$ there exists $T_\epsilon : \mathcal{X} \rightarrow \mathcal{Y}$ satisfying $T \# \mathbb{P} = \pi_y^*$ and $\int_{\mathcal{X}} c(x, T_\epsilon(x)) d\mathbb{P}(x) < \text{Cost}_w(\mathbb{P}, \mathbb{Q}) + \epsilon$. It remains to substitute this T_ϵ to Monge's IT problem (11) to get an ϵ -close transport cost to Kantorovich's IT cost (12). As this works for every $\epsilon > 0$, we conclude that min in (12) is the same as inf in (11). \square

Proof of Proposition 2. To begin with, we prove that $\Pi^w(\mathbb{P}, \mathbb{Q})$ is a weak-* compact set. Pick any sequence $\pi_n \in \Pi^w(\mathbb{P}, \mathbb{Q})$. It is bounded as all π_n are probability measures ($\|\pi_n\|_1 = 1$). Hence by the Banach-Alaoglu theorem (Santambrogio, 2015, Box 1.2), there exists a subsequence π_{n_k} weakly-* converging to some $\pi \in \mathcal{M}(\mathcal{X} \times \mathcal{Y})$. It remains to check that $\pi \in \Pi^w(\mathbb{P}, \mathbb{Q})$. Let (μ_{n_k}, ν_{n_k}) denote the marginals of π_{n_k} and (μ, ν) be the marginals of π . Pick any $f \in \mathcal{C}(\mathcal{Y})$ with $f \leq 0$. Since $\pi_{n_k} \in \Pi^w(\mathbb{P}, \mathbb{Q})$, it holds that $0 \leq \nu_{n_k} \leq w\mathbb{Q}$, $w \int_{\mathcal{Y}} f(y) d\mathbb{Q}(y) \leq \int_{\mathcal{Y}} f(y) d\nu_{n_k}(y) \leq 0$ (Lemma 1). We have

$$\int_{\mathcal{Y}} f(y) d\nu(y) = \int_{\mathcal{X} \times \mathcal{Y}} f(y) d\pi(x, y) = \lim_{k \rightarrow \infty} \int_{\mathcal{X} \times \mathcal{Y}} f(y) d\pi_{n_k}(x, y) = \lim_{k \rightarrow \infty} \int_{\mathcal{Y}} f(y) d\nu_{n_k}(y).$$

The latter limit is $\geq w \int_{\mathcal{Y}} f(y) d\mathbb{Q}(y)$ and ≤ 0 . As this holds for every continuous $f \leq 0$, we conclude that $0 \leq \nu \leq w\mathbb{Q}$. By the analogous analysis one may prove that $\mu = \mathbb{P}$ and $\pi \geq 0$. Thus, $\pi \in \Pi^w(\mathbb{P}, \mathbb{Q})$ and $\Pi^w(\mathbb{P}, \mathbb{Q})$ is a weak-* compact.

The functional $\pi \mapsto \int_{\mathcal{X} \times \mathcal{Y}} c(x, y) d\pi(x, y)$ is continuous in the space $\mathcal{M}(\mathcal{X} \times \mathcal{Y})$ equipped with weak-* topology because $c : \mathcal{X} \times \mathcal{Y} \rightarrow \mathbb{R}$ is continuous. Since $\Pi^w(\mathbb{P}, \mathbb{Q})$ is a compact set, there exists $\pi^* \in \Pi^w(\mathbb{P}, \mathbb{Q})$ attaining the minimum on $\Pi^w(\mathbb{P}, \mathbb{Q})$. This follows from the Weierstrass extreme value theorem and ends the proof. \square

Bibliographical remark. The results showing the existence of minimizers π^* in partial OT (4) already exist, see (Caffarelli & McCann, 2010, Lemma 2.2) or (Figalli, 2010, §2). They also provide the existence of minimizers in our IT problem (12). Yet, the authors study the particular case when \mathbb{P}, \mathbb{Q} have densities on $\mathcal{X}, \mathcal{Y} \subset \mathbb{R}^D$. For *completeness*, we include a separate proof of existence as we do not require the absolute continuity assumption. The proof is performed via the usual technique based on weak-* compactness in dual spaces and is analogous to (Santambrogio, 2015, Theorem 1.4) which proves the existence of minimizers for OT problem (2). Our proof is slightly more technical due to the inequality constraint.

Proof of Theorem 2. The fact that $w \mapsto \text{Cost}_w(\mathbb{P}, \mathbb{Q})$ is non-increasing follows from the inclusion $\Pi^{w_1}(\mathbb{P}, \mathbb{Q}) \subset \Pi^{w_2}(\mathbb{P}, \mathbb{Q})$ for $w_1 \leq w_2$. This inclusion means that for larger values of w , the minimization in (12) is performed over a larger set of admissible plans. As for convexity, take any IT plans $\pi^{w_1} \in \Pi^{w_1}(\mathbb{P}, \mathbb{Q})$, $\pi^{w_2} \in \Pi^{w_2}(\mathbb{P}, \mathbb{Q})$ for w_1, w_2 , respectively. For any $\alpha \in [0, 1]$ consider the mixture $\pi' = \alpha\pi^{w_1} + (1 - \alpha)\pi^{w_2}$. Note that $\pi'_y = \alpha\pi_y^{w_1} + (1 - \alpha)\pi_y^{w_2} \leq \alpha w_1 \mathbb{Q} + (1 - \alpha)w_2 \mathbb{Q} = (\alpha w_1 + (1 - \alpha)w_2)\mathbb{Q}$. Therefore, $\pi' \in \Pi^{\alpha w_1 + (1 - \alpha)w_2}(\mathbb{P}, \mathbb{Q})$. We derive

$$\begin{aligned} \text{Cost}_{\alpha w_1 + (1 - \alpha)w_2}(\mathbb{P}, \mathbb{Q}) &\leq \int_{\mathcal{X} \times \mathcal{Y}} c(x, y) d\pi'(x, y) = \\ &\alpha \int_{\mathcal{X} \times \mathcal{Y}} c(x, y) d\pi^{w_1}(x, y) + (1 - \alpha) \int_{\mathcal{X} \times \mathcal{Y}} c(x, y) d\pi^{w_2}(x, y) = \\ &\alpha \text{Cost}_{w_1}(\mathbb{P}, \mathbb{Q}) + (1 - \alpha) \text{Cost}_{w_2}(\mathbb{P}, \mathbb{Q}), \end{aligned} \quad (21)$$

which shows the convexity of $w \mapsto \text{Cost}_w(\mathbb{P}, \mathbb{Q})$.

Now we prove that $\lim_{w \rightarrow \infty} \text{Cost}_w(\mathbb{P}, \mathbb{Q}) = \text{Cost}_\infty(\mathbb{P}, \mathbb{Q})$. For every $w \geq 1$ and $\pi \in \Pi^w(\mathbb{P}, \mathbb{Q})$, it holds that $\pi_y \leq w\mathbb{Q}$. This means that $\text{Supp}(\pi_y) \subset \text{Supp}(\mathbb{Q})$. As a result, we see that $\Pi^w(\mathbb{P}, \mathbb{Q}) \subset \Pi^\infty(\mathbb{P}, \mathbb{Q})$, i.e., $\text{Cost}_w(\mathbb{P}, \mathbb{Q}) \geq \text{Cost}_\infty(\mathbb{P}, \mathbb{Q})$. We already know that $w \mapsto \text{Cost}_w(\mathbb{P}, \mathbb{Q})$ is non-increasing, so it suffices to show that for every $\epsilon > 0$ there exists $w = w(\epsilon) \in [1, +\infty)$ such that $\text{Cost}_w(\mathbb{P}, \mathbb{Q}) \leq \text{Cost}_\infty(\mathbb{P}, \mathbb{Q}) + \epsilon$. This will provide that $\lim_{w \rightarrow \infty} \text{Cost}_w(\mathbb{P}, \mathbb{Q}) = \text{Cost}_\infty(\mathbb{P}, \mathbb{Q})$.

Pick any $\epsilon > 0$. Consider the set $\mathcal{S} \stackrel{\text{def}}{=} \{(x, y) \in \mathcal{X} \times \mathcal{Y} \text{ such that } y \in \text{NN}(x)\}$. It is a compact set. To see this, we pick any sequence $(x_n, y_n) \in \mathcal{S}$. It is contained in compact $\mathcal{X} \times \mathcal{Y}$. Therefore, it has a sub-sequence (x_{n_k}, y_{n_k}) converging to some $(x, y) \in \mathcal{X} \times \mathcal{Y}$. It remains to check that $(x, y) \in \mathcal{S}$. Since $\text{Supp}(\mathbb{Q})$ is compact and $y_{n_k} \in \text{NN}(x_{n_k}) \subset \text{Supp}(\mathbb{Q})$, we have $y \in \text{Supp}(\mathbb{Q})$ as well. At the same time, by the continuity of c^* (Proposition 1) and c , we have

$$c(x, y) - c^*(x) = \lim_{k \rightarrow \infty} \{c(x_{n_k}, y_{n_k}) - c^*(x_{n_k})\} = \lim_{k \rightarrow \infty} 0 = 0,$$

which means that $y \in \text{NN}(x)$ and $(x, y) \in \mathcal{S}$, i.e., \mathcal{S} is compact.

Since $(x, y) \mapsto c(x, y) - c^*(x)$ is a continuous function, for each $(x, y) \in \mathcal{S}$ there exists an open neighborhood $U_x \times V_y \subset \mathcal{X} \times \mathcal{Y}$ of (x, y) such that for all $(x', y') \in U_x \times V_y$ it holds that $c(x', y') - c^*(x') < \epsilon$ or, equivalently, $c(x', y') < c^*(x') + \epsilon$. Since $\bigcup_{(x, y) \in \mathcal{S}} U_x \times V_y$ is an open coverage of the compact set \mathcal{S} , there exists a finite sub-coverage $\bigcup_{n=1}^N U_{x_n} \times V_{y_n}$ of \mathcal{S} .

In particular, $\mathcal{X} = \bigcup_{n=1}^N V_{x_n}$. For convenience, we simplify the notation and put $U_n \stackrel{\text{def}}{=} U_{x_n}$ and $V_n \stackrel{\text{def}}{=} V_{y_n}$. Now we put $U'_1 \stackrel{\text{def}}{=} U_1$ and iteratively define $U'_n \stackrel{\text{def}}{=} U_n \setminus U'_{n-1}$ for $n \geq 2$. By the construction, it holds that the entire space \mathcal{X} is a disjoint union of U'_n , i.e., $\mathcal{X} = \bigsqcup_{n=1}^N U'_n$. Some of U'_n may be empty, so we just remove them from the sequence and for convenience assume that each U'_n is not empty. Now consider the measure $\pi \in \mathcal{P}(\mathcal{X} \times \mathcal{Y})$ which is given by

$$\pi \stackrel{\text{def}}{=} \sum_{n=1}^N [\mathbb{P}|_{U'_n} \times \frac{\mathbb{Q}|_{V_n}}{\mathbb{Q}(V_n)}]. \quad (22)$$

Here for $\mu, \nu \in \mathcal{M}_+(\mathcal{X}), \mathcal{M}_+(\mathcal{Y})$, we use \times to denote their product measure $\mu \times \nu \in \mathcal{M}(\mathcal{X} \times \mathcal{Y})$. In turn, for a measurable $A \subset \mathcal{X}$, we use $\mu|_A$ to denote the restriction of μ to A , i.e., measure $\mu' \in \mathcal{M}(\mathcal{X})$ satisfying $\mu'(B) = \mu(A \cap B)$ for every measurable $B \subset \mathcal{X}$. Note that $\sum_{n=1}^N \mathbb{P}|_{U'_n} = \mathbb{P}$ and $\sum_{n=1}^N \mathbb{P}(U'_n) = \sum_{n=1}^N \mathbb{P}|_{U'_n}(U'_n) = 1$ by the construction of U'_n . At the same time, for each n it holds that $\frac{\mathbb{Q}|_{V_n}}{\mathbb{Q}(V_n)}$ is a probability measure because of the normalization $\mathbb{Q}(V_n)$. Note that this normalization is necessarily positive because V_n is a neighborhood of a point in $\text{Supp}(\mathbb{Q})$. Therefore, since sets U'_n are disjoint and cover \mathcal{X} , we have $\pi_x = \sum_{n=1}^N \mathbb{P}|_{U'_n} = \mathbb{P}$. Now let us show that there exists w such that $\pi_y \leq w\mathbb{Q}$. It suffices to take $w = \sum_{n=1}^N \frac{\mathbb{P}(U'_n)}{\mathbb{Q}(V_n)}$. Indeed, in this case for every measurable $A \subset \mathcal{X}$ we have

$$\pi_y(A) = \sum_{n=1}^N \mathbb{P}(U'_n) \frac{\mathbb{Q}(A \cap U'_n)}{\mathbb{Q}(V_n)} \leq \sum_{n=1}^N \mathbb{P}(U'_n) \frac{\mathbb{Q}(A)}{\mathbb{Q}(V_n)} \leq \mathbb{Q}(A) \sum_{n=1}^N \frac{\mathbb{P}(U'_n)}{\mathbb{Q}(V_n)} \leq w\mathbb{Q}(A),$$

which yields $\pi_y \leq w\mathbb{Q}$ and means that $\pi \in \Pi^w(\mathbb{P}, \mathbb{Q})$ for our chosen w . Now let us compute the cost of π :

$$\begin{aligned} \int_{\mathcal{X} \times \mathcal{Y}} c(x, y) d\pi(x, y) &= \sum_{n=1}^N \int_{U'_n} \left\{ \frac{1}{\mathbb{Q}(V_n)} \int_{V_n} c(x, y) d\mathbb{Q}|_{V_n}(y) \right\} d\mathbb{P}|_{U'_n}(x) \leq \\ &\sum_{n=1}^N \int_{U'_n} \underbrace{\left\{ \frac{1}{\mathbb{Q}(V_n)} \int_{V_n} (c^*(x) + \epsilon) d\mathbb{Q}|_{V_n}(y) \right\}}_{=c^*(x) + \epsilon} d\mathbb{P}|_{U'_n}(x) = \sum_{n=1}^N \int_{U'_n} (c^*(x) + \epsilon) d\mathbb{P}|_{U'_n}(x) = \\ &\int_{\mathcal{X}} (c^*(x) + \epsilon) d\mathbb{P}(x) = \text{Cost}_\infty(\mathbb{P}, \mathbb{Q}) + \epsilon. \end{aligned} \quad (23)$$

To finish the proof it remains to note that this plan is not necessarily a minimizer for (12), i.e., $\int_{\mathcal{X} \times \mathcal{Y}} c(x, y) d\pi(x, y)$ is an upper bound on $\text{Cost}_w(\mathbb{P}, \mathbb{Q})$. Therefore, we have $\text{Cost}_w(\mathbb{P}, \mathbb{Q}) \leq \text{Cost}_\infty(\mathbb{P}, \mathbb{Q}) + \epsilon$ for our chosen $w = w(\epsilon)$. \square

Bibliographical remark. There exist seemingly related **but actually different results** in the fundamental OT literature, see (Figalli, 2010, Lemma 2.1) or (Caffarelli & McCann, 2010, §3). There the authors study partial OT problem (4) and study how the partial OT plan and OT cost evolve when the marginals $w_0\mathbb{P}$ and $w_1\mathbb{Q}$ are fixed and the required mass amount to transport changes from 0 to $\min\{w_0, w_1\}$. In our study, the first marginal $w_0\mathbb{P}$ and the amount of mass to transport m are fixed ($w_0 = m = 1$), and we study how the OT cost changes when $w_1 \rightarrow \infty$ in the IT problem.

Proof of Theorem 3. Note that $\mathcal{P}(\mathcal{X} \times \mathcal{Y})$ is (weak-*) compact. This can be derived from the Banach-Alaoglu theorem analogously to the compactness of $\Pi^w(\mathbb{P}, \mathbb{Q})$ in the proof of Theorem (2). Therefore, *any* sequence in $\mathcal{P}(\mathcal{X} \times \mathcal{Y})$ has a converging sub-sequence. In our case, for brevity, we assume that $\pi^{w_n} \in \Pi^{w_n}(\mathbb{P}, \mathbb{Q})$ itself weakly-* converges to some $\pi^* \in \mathcal{P}(\mathcal{X} \times \mathcal{Y})$. Since $\pi_x^{w_n} = \mathbb{P}$ for all n , we also have $\pi_x^* = \mathbb{P}$. As $\lim_{n \rightarrow \infty} w_n = \infty$, we conclude from Theorem 2 that

$$\text{Cost}_\infty(\mathbb{P}, \mathbb{Q}) = \lim_{n \rightarrow \infty} \text{Cost}_{w_n}(\mathbb{P}, \mathbb{Q}) = \lim_{n \rightarrow \infty} \int_{\mathcal{X} \times \mathcal{Y}} c(x, y) d\pi^{w_n}(x, y) = \int_{\mathcal{X} \times \mathcal{Y}} c(x, y) d\pi^*(x, y), \quad (24)$$

where the last equality holds since π^{w_n} (weakly-*) converges to π^* . From (24), we see that the cost of π^* is perfect and it remains to check that $\text{Supp}(\pi_y^*) \subset \text{Supp}(\mathbb{Q})$. Assume the opposite and pick any $y^* \in \text{Supp}(\pi_y^*)$ such that $y^* \notin \text{Supp}(\mathbb{Q})$. By the definition of the support, there exists $\epsilon > 0$ and a neighborhood $U = \{y \in \mathcal{Y} \text{ such that } \|y - y^*\|_{\mathcal{Y}} < \epsilon\}$ of y^* satisfying $\pi_y^*(U) > 0$ and $U \cap \text{Supp}(\mathbb{Q}) = \emptyset$. Let $h(y) \stackrel{\text{def}}{=} \max\{0, \epsilon - \|y - y^*\|_{\mathcal{Y}}\}$. From $\pi_y^{w_n} \leq w_n \mathbb{Q}$ (for all n), it follows that $\text{Supp}(\pi_y^{w_n}) \subset \text{Supp}(\mathbb{Q})$. Therefore, $\pi_y^{w_n}(U) = 0$ for all n . Since π^{w_n} converges to π^* , we have

$$\lim_{n \rightarrow \infty} \int_{\mathcal{Y}} h(y) d\pi^{w_n}(y) = \int_{\mathcal{Y}} h(y) d\pi^*(y). \quad (25)$$

The left part is zero because $h(y)$ vanishes outside U and $\int_U h(y) d\pi^{w_n}(y) = 0$ as $\pi_y^{w_n}(U) = 0$. The right part equals $\int_U h(y) d\pi^*(y)$ and is positive as $\pi^*(U) > 0$ and $h(y) > 0$ for $y \in U$. This is a contradiction. Therefore, $\text{Supp}(\pi_y^*) \subset \text{Supp}(\mathbb{Q})$. Now we see that $\pi^* \in \Pi^\infty(\mathbb{P}, \mathbb{Q})$ is a perfect plan as its cost matches the perfect cost. \square

Proof of Theorem 4. Let $\Pi(\mathbb{P}) \subset \mathcal{P}(\mathcal{X} \times \mathcal{Y})$ denote the subset of probability measures $\pi \in \mathcal{P}(\mathcal{X} \times \mathcal{Y})$ satisfying $\pi_x = \mathbb{P}$. Consider a functional $I : \Pi(\mathbb{P}) \rightarrow \{0, +\infty\}$ defined by $I(\pi) \stackrel{\text{def}}{=} \sup_{f \leq 0} \int_{\mathcal{Y}} f(y) d(w\mathbb{Q} - \pi_y)(y)$, where the sup is taken over non-positive $f \in \mathcal{C}(\mathcal{Y})$. From Lemma 1, we have $I(\pi) = 0$ when $\pi \in \Pi^w(\mathbb{P}, \mathbb{Q})$ and $I(\pi) = +\infty$ otherwise. Indeed, if there exists a non-positive function satisfying $\int_{\mathcal{Y}} f(y) d(w\mathbb{Q} - \pi_y)(y) > 0$, then function Cf (for $C > 0$) also satisfies this condition and provides C -times bigger value which tends to ∞ with $C \rightarrow \infty$. We use $I(\pi)$ incorporate the right constraint $\pi_y \leq w\mathbb{Q}$ in $\pi \in \Pi^w(\mathbb{P}, \mathbb{Q})$ to the objective and obtain the equivalent to (12) problem:

$$\begin{aligned} \min_{\pi \in \Pi^w(\mathbb{P}, \mathbb{Q})} \int_{\mathcal{X} \times \mathcal{Y}} c(x, y) d\pi(x, y) &= \min_{\pi \in \Pi(\mathbb{P})} \left\{ \int_{\mathcal{X} \times \mathcal{Y}} c(x, y) d\pi(x, y) + I(\pi) \right\} = \\ &= \min_{\pi \in \Pi(\mathbb{P})} \left\{ \int_{\mathcal{X} \times \mathcal{Y}} c(x, y) d\pi(x, y) + \sup_{f \leq 0} \int_{\mathcal{Y}} f(y) d(w\mathbb{Q} - \pi_y)(y) \right\} = \\ &= \min_{\pi \in \Pi(\mathbb{P})} \sup_{f \leq 0} \left\{ \int_{\mathcal{X} \times \mathcal{Y}} c(x, y) d\pi(x, y) + \int_{\mathcal{Y}} f(y) d(w\mathbb{Q} - \pi_y)(y) \right\} = \end{aligned} \quad (26)$$

$$\sup_{f \leq 0} \min_{\pi \in \Pi(\mathbb{P})} \left\{ \int_{\mathcal{X} \times \mathcal{Y}} c(x, y) d\pi(x, y) + \int_{\mathcal{Y}} f(y) d(w\mathbb{Q} - \pi_y)(y) \right\} = \quad (27)$$

$$\begin{aligned} \sup_{f \leq 0} \left\{ \min_{\pi \in \Pi(\mathbb{P})} \left\{ \int_{\mathcal{X} \times \mathcal{Y}} c(x, y) d\pi(x, y) - \int_{\mathcal{Y}} f(y) d\pi_y(y) \right\} + w \int_{\mathcal{Y}} f(y) d\mathbb{Q}(y) \right\} = \\ \sup_{f \leq 0} \left\{ \min_{\pi \in \Pi(\mathbb{P})} \left\{ \int_{\mathcal{X} \times \mathcal{Y}} c(x, y) d\pi(x, y) - \int_{\mathcal{X} \times \mathcal{Y}} f(y) d\pi(x, y) \right\} + w \int_{\mathcal{Y}} f(y) d\mathbb{Q}(y) \right\} = \end{aligned} \quad (28)$$

$$\sup_{f \leq 0} \left\{ \min_{\pi \in \Pi(\mathbb{P})} \left\{ \int_{\mathcal{X}} \int_{\mathcal{Y}} c(x, y) d\pi(y|x) \underbrace{d\mathbb{P}(x)}_{=d\pi_x(x)} - \int_{\mathcal{X}} \int_{\mathcal{Y}} f(y) d\pi(y|x) \underbrace{d\mathbb{P}(x)}_{=d\pi_x(x)} \right\} + w \int_{\mathcal{Y}} f(y) d\mathbb{Q}(y) \right\} = \quad (29)$$

$$\sup_{f \leq 0} \left\{ \min_{\pi \in \Pi(\mathbb{P})} \left\{ \int_{\mathcal{X}} \int_{\mathcal{Y}} (c(x, y) - f(y)) d\pi(y|x) d\mathbb{P}(x) \right\} + w \int_{\mathcal{Y}} f(y) d\mathbb{Q}(y) \right\} \quad (30)$$

In transition from (26) to (27) we use the minimax theorem to swap sup and min (Terkelsen, 1972, Corollary 2). This is possible because the expression in (26) is a bilinear functional of (π, f) . Thus, it is convex in π and concave in f . At the same time, $\Pi(\mathbb{P})$ is a convex and (weak-*) compact set. The latter can be derived analogously to the compactness of $\Pi^w(\mathbb{P}, \mathbb{Q})$ in the proof of Theorem 2. In transition from (28) to (29), we use the measure disintegration theorem to represent $d\pi(x, y)$ as the marginal $d\pi_x(x) = d\mathbb{P}(x)$ and a family of conditional measures $d\pi(y|x)$ on \mathcal{Y} . We note that

$$\min_{\pi \in \Pi(\mathbb{P})} \int_{\mathcal{X}} \int_{\mathcal{Y}} (c(x, y) - f(y)) d\pi(y|x) d\mathbb{P}(x) \geq \int_{\mathcal{X}} \underbrace{\min_{y \in \mathcal{Y}} (c(x, y) - f(y))}_{=f^c(x)} d\mathbb{P}(x). \quad (31)$$

On the other hand, consider the measurable selection $T : \mathcal{X} \rightarrow \mathcal{Y}$ for the set-valued map $x \mapsto \arg \min_{y \in \mathcal{Y}} (c(x, y) - f(y))$. It exists thanks to (Aliprantis & Border, 2006, Theorem 18.19). As a result, for the deterministic plan $\pi^T = [\text{id}, T]_{\#} \mathbb{P}$, the minimum in (31) is indeed attained. Therefore, (31) is the equality. We combine (30) and (31) and obtain

$$\text{Cost}_w(\mathbb{P}, \mathbb{Q}) = \min_{\pi \in \Pi^w(\mathbb{P}, \mathbb{Q})} \int_{\mathcal{X} \times \mathcal{Y}} c(x, y) d\pi(x, y) = \sup_{f \leq 0} \left\{ \int_{\mathcal{X}} f^c(x) d\mathbb{P}(x) + w \int_{\mathcal{Y}} f(y) d\mathbb{Q}(y) \right\}. \quad (32)$$

It remains to prove that sup in the right part is actually attained at some non-positive $f^* \in \mathcal{C}(\mathcal{Y})$. Let $f_1, f_2, \dots \in \mathcal{C}(\mathcal{Y})$ be a sequence of non-positive functions for which $\lim_{n \rightarrow \infty} \left\{ \int_{\mathcal{X}} f_n^c(x) d\mathbb{P}(x) + w \int_{\mathcal{Y}} f_n(y) d\mathbb{Q}(y) \right\} = \text{Cost}_w(\mathbb{P}, \mathbb{Q})$. For $g \in \mathcal{C}(\mathcal{X})$, we define the $(c, -)$ -transform $g^{(c, -)}(y) \stackrel{\text{def}}{=} \min_{x \in \mathcal{X}} [\min(c(x, y) - g(x)), 0] \leq 0$. It yields a (uniformly) continuous non-positive function satisfying $|g^{(c, -)}(y) - g^{(c, -)}(y')| \leq \omega(\|y - y'\|_{\mathcal{Y}})$, where ω is the modulus of continuity of $c(x, y)$. This statement can be derived analogously to the proof of Proposition 1.

Before going further, let us highlight two important facts which we are going to use below. Consider any $g \in \mathcal{C}(\mathcal{X})$ and $0 \geq h \in \mathcal{C}(\mathcal{Y})$ satisfying $g(x) + h(y) \leq c(x, y)$ for all $(x, y) \in \mathcal{X} \times \mathcal{Y}$. First, from the definition of $(c, -)$ -transform, one can see that for all $(x, y) \in \mathcal{X} \times \mathcal{Y}$ it holds that $0 \geq g^{(c, -)} \geq h$ and

$$g(x) + h(y) \leq g(x) + g^{(c, -)}(y) \leq c(x, y), \quad (33)$$

i.e., $(g, g^{(c, -)})$ also satisfies the assumptions of (g, h) . Second, from the definition of c -transform, it holds that $h^c \geq g$ and

$$g(x) + h(y) \leq h^c(x) + h(y) \leq c(x, y), \quad (34)$$

i.e., the pair (h^c, h) satisfies the same assumptions as (g, h) .

Now we get back to our sequence f_1, f_2, \dots . For each n and $(x, y) \in \mathcal{X} \times \mathcal{Y}$, we have $f_n^c(x) + f_n(y) \leq c(x, y)$. Next,

$$f_n^c(x) + f_n(y) \leq f_n^c(x) + (f_n^{(c, -)})^c(y) \leq ((f_n^c)^{(c, -)})^c(x) + (f_n^{(c, -)})(y) \quad [\leq c(x, y)], \quad (35)$$

where we first used (33) with $(g, h) = (f_n^c, f_n)$ and then used (34) with $(g, h) = (f_n^c, (f_n^{(c, -)})^c)$. In particular, we have $f_n^c \leq ((f_n^c)^{(c, -)})^c$ and $f_n \leq (f_n^{(c, -)})^c$. We sum these inequalities with weights 1 and w , and for all $(x, y) \in \mathcal{X} \times \mathcal{Y}$ obtain

$$f_n^c(x) + w f_n(y) \leq ((f_n^c)^{(c, -)})^c(x) + w (f_n^{(c, -)})^c(y) = h_n^c(x) + w h_n(y), \quad (36)$$

where for convenience we denote $h_n \stackrel{\text{def}}{=} (f_n^{(c, -)})^c$. Integrating (36) with $(x, y) \sim \mathbb{P} \times \mathbb{Q}$ yields

$$\int_{\mathcal{X}} f_n^c(x) d\mathbb{P}(x) + w \int_{\mathcal{Y}} f_n(y) d\mathbb{Q}(y) \leq \int_{\mathcal{X}} h_n^c(x) d\mathbb{P}(x) + w \int_{\mathcal{Y}} h_n(y) d\mathbb{Q}(y). \quad (37)$$

This means that potential h_n provides not smaller dual objective value than f_n . As a result, sequence h_1, h_2, \dots also satisfies $\lim_{n \rightarrow \infty} \left\{ \int_{\mathcal{X}} h_n^c(x) d\mathbb{P}(x) + w \int_{\mathcal{Y}} h_n(y) d\mathbb{Q}(y) \right\} = \text{Cost}_w(\mathbb{P}, \mathbb{Q})$. Now we forget about f_1, f_2, \dots and work with h_1, h_2, \dots .

All the functions h_n are uniformly equicontinuous as they share the same modulus of continuity ω because they are $(c, -)$ -transforms by their definition. Let $v_n(y) \stackrel{\text{def}}{=} h_n(y) - \max_{y' \in \mathcal{Y}} h_n(y')$. This function is also non-positive and uniformly continuous as well. Note that v_n provides the same dual objective value as h_n . This follows from the definition of $v^c = h^c + \max_{y' \in \mathcal{Y}} h_n(y')$. Here the additive constant vanishes, i.e., $v_n^c(x) + v_n(y) = h_n^c(x) + h_n(y)$. At the same time, v_n are all uniformly bounded. Indeed, let $y_n \in \mathcal{Y}$ be any point where $v_n(y_n) = 0$. Then for all $y \in \mathcal{Y}$ it holds that $|v_n(y)| = |v_n(y) - v_n(y_n)| \leq \omega(\|y - y_n\|_{\mathcal{Y}}) \leq \omega(\text{diam}(\mathcal{Y}))$. Therefore, by the Arzelà–Ascoli theorem, there exists a subsequence v_{n_k} uniformly converging to some $f^* \in \mathcal{C}(\mathcal{Y})$. As all $v_{n_k} \leq 0$, it holds that $f^* \leq 0$ as well. It remains to check that f^* attains the supremum in (32).

To begin with, we prove that $v_{n_k}^c$ uniformly converges to $(f^*)^c$. Denote $\|v_{n_k} - f^*\|_{\infty} = \epsilon_k$. For all $(x, y) \in \mathcal{X} \times \mathcal{Y}$, we have

$$c(x, y) - f^*(y) - \epsilon_k \leq c(x, y) - v_{n_k}(y) \leq c(x, y) - f^*(y) + \epsilon_k \quad (38)$$

since $|v_{n_k}(y) - f^*(y)| \leq \|v_{n_k} - f^*\|_\infty < \epsilon$. We take $\min_{y \in \mathcal{Y}}$ in (38) and obtain $(f^*)^c(x) - \epsilon_k \leq v_{n_k}^c(x) \leq (f^*)^c(x) + \epsilon_k$. As this holds for all $x \in \mathcal{X}$, we have just proved that $\|v_{n_k}^c - (f^*)^c\|_\infty < \epsilon_k$. This means that $v_{n_k}^c$ uniformly converges to $(f^*)^c$ as well since $\lim_{k \rightarrow \infty} \|v_{n_k} - f^*\|_\infty = \lim_{k \rightarrow \infty} \epsilon_k = 0$. Thanks to the uniform convergence, we have

$$\text{Cost}_w(\mathbb{P}, \mathbb{Q}) = \lim_{k \rightarrow \infty} \left\{ \int_{\mathcal{X}} (v_{n_k})^c(x) d\mathbb{P}(x) + \int_{\mathcal{Y}} v_{n_k}(y) d\mathbb{Q}(y) \right\} = \int_{\mathcal{X}} (f^*)^c(x) d\mathbb{P}(x) + \int_{\mathcal{Y}} f^*(y) d\mathbb{Q}(y). \quad (39)$$

We conclude that f^* is a maximizer of (32) that we seek for. \square

Bibliographical remark. There exists a duality formula for partial OT (4), see (Caffarelli & McCann, 2010, §2) which can be reduced to duality formula to IT problem (12). However, it is hard to relate the resulting formula with ours (13). We do not know how to derive one formula from the other. More importantly, it is unclear how to turn their formula to the computational algorithm. Our formula provides an opportunity to do this by using the saddle point reformulation of the dual problem which nowadays becomes standard for neural OT, see (Korotin et al., 2022c; Fan et al., 2021; Rout et al., 2021). We will give further comments after the next proof. The second part of the derivation of our formula (existence of a maximizer f^*) is inspired by the (Santambrogio, 2015, Proposition 1.11) which shows the existence of maximizers for standard OT (2).

Proof of Theorem 5. By the definition of f^* , we have

$$\text{Cost}_w(\mathbb{P}, \mathbb{Q}) = \min_{T: \mathcal{X} \rightarrow \mathcal{Y}} \mathcal{L}(f^*, T) = \min_{T: \mathcal{X} \rightarrow \mathcal{Y}} \int_{\mathcal{X}} \{c(x, T(x)) - f^*(T(x))\} d\mathbb{P}(x) + w \int_{\mathcal{Y}} f^*(y) d\mathbb{Q}(y) \leq \quad (40)$$

$$\int_{\mathcal{X}} \{c(x, T^*(x)) - f^*(T^*(x))\} d\mathbb{P}(x) + w \int_{\mathcal{Y}} f^*(y) d\mathbb{Q}(y) = \quad (41)$$

$$\begin{aligned} & \int_{\mathcal{X}} c(x, T^*(x)) d\mathbb{P}(x) - \int_{\mathcal{X}} f^*(y) d[T^* \# \mathbb{P}](y) + w \int_{\mathcal{Y}} f^*(y) d\mathbb{Q}(y) = \\ & \text{Cost}_w(\mathbb{P}, \mathbb{Q}) + \underbrace{\int_{\mathcal{Y}} f^*(y) d[w\mathbb{Q} - T^* \# \mathbb{P}](y)}_{\leq 0 \text{ (Lemma 1)}} \leq \text{Cost}_w(\mathbb{P}, \mathbb{Q}). \end{aligned} \quad (42)$$

This means that all the inequalities in (40)-(42) are equalities. Since (40) equals (41), we have $T^* \in \arg \min_{T: \mathcal{X} \rightarrow \mathcal{Y}} \mathcal{L}(f^*, T)$. \square

Bibliographic remark (theoretical part). The idea of the theorem is similar to that of (Rout et al., 2021, Lemma 4.2), (Gazdieva et al., 2022, Lemma 3), (Korotin et al., 2022c, Lemma 4), (Fan et al., 2021, Theorem 2) which prove that their respective saddle point objectives $\max_f \min_T \mathcal{L}(f, T)$ can be used to recover optimal T^* from *some* optimal saddle points (f^*, T^*) . Our functional (15) differs, and we have the constraint $f \leq 0$. We again emphasize here that not for all the saddle points (f^*, T^*) it necessarily holds that T^* is the IT map, see the discussion in limitations (Appendix A).

Bibliographic remark (algorithmic part). To derive our saddle point optimization problem (15), we use the c -transform expansion proposed by (Nhan Dam et al., 2019) in the context of Wasserstein GANs and later explored by (Korotin et al., 2021b; 2022c; Rout et al., 2021; Fan et al., 2021; Gazdieva et al., 2022; Henry-Labordere, 2019) in the context of learning OT maps. That is, our resulting algorithm 1 overlaps with the standard maximin neural OT solver, see, e.g., (Gazdieva et al., 2022, Algorithm 1). The difference is in the constraint $f \leq 0$ and the additional multiplier $w \geq 1$.

Proof of Proposition 4. From the proof of Theorem 5, we see that $\int_{\mathcal{Y}} f^*(y) d[w\mathbb{Q} - T^* \# \mathbb{P}](y) = 0$. Recall that $f^* \leq 0$. This means that $f(y) = 0$ for $y \in \text{Supp}(w\mathbb{Q} - T^* \# \mathbb{P})$. Indeed, assume the opposite, i.e., there exists some $y \in \text{Supp}(w\mathbb{Q} - T^* \# \mathbb{P})$ for which $f(y) < 0$. In this case, the same holds for all y' in a small neighborhood U of y as f is continuous. At the same time, $\int_{\mathcal{Y}} f^*(y) d[w\mathbb{Q} - T^* \# \mathbb{P}](y) \leq \int_U f^*(y) d[w\mathbb{Q} - T^* \# \mathbb{P}](y) < 0$ since $[w\mathbb{Q} - T^* \# \mathbb{P}]$ is a non-negative measure satisfying $[w\mathbb{Q} - T^* \# \mathbb{P}](U) > 0$ by the definition of the support. This is a contradiction. To finish the proof it remains to note that $\text{Supp}(\mathbb{Q}) \setminus \text{Supp}(T^* \# \mathbb{P}) \subset \text{Supp}(w\mathbb{Q} - T^* \# \mathbb{P})$, i.e., $f(y) = 0$ for $y \in \text{Supp}(\mathbb{Q}) \setminus \text{Supp}(T^* \# \mathbb{P})$ as well. \square

Bibliographical remark. Treating functional $\mathcal{L}(f, T)$ in (16) as a Lagrangian, Proposition 4 can be viewed as a consequence of the complementary slackness in the Karush-Kuhn-Tucker conditions (Karush, 2014).

F. Additional Experimental Results

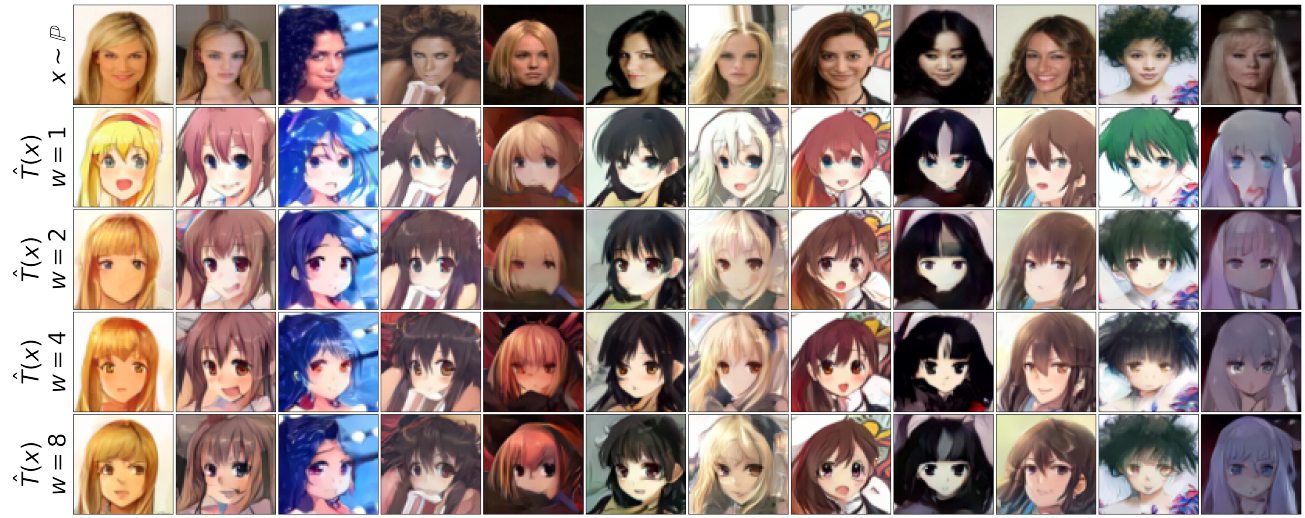
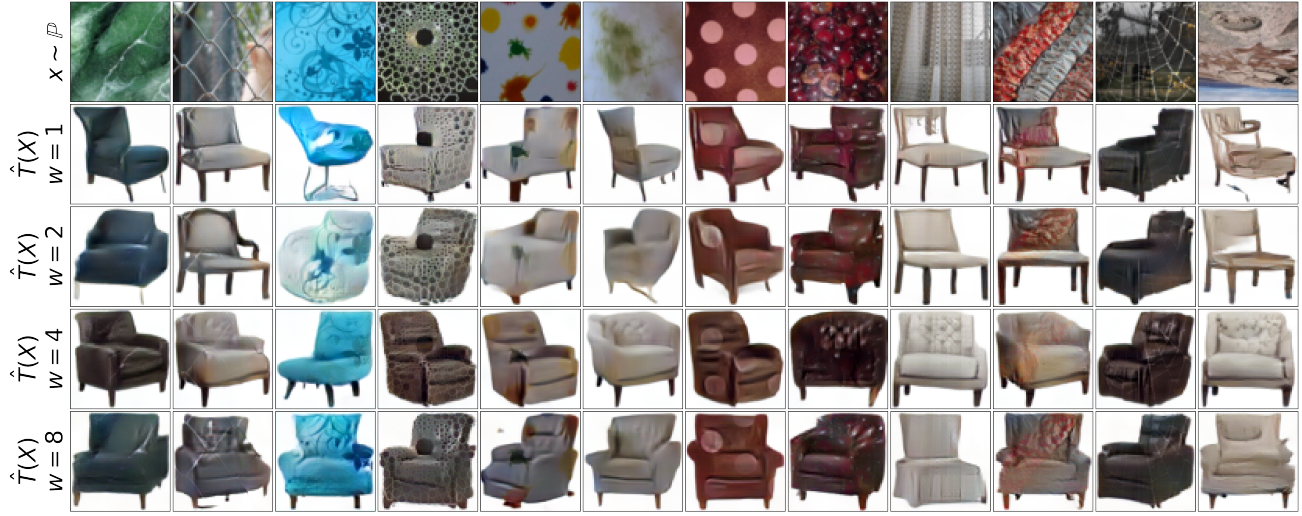
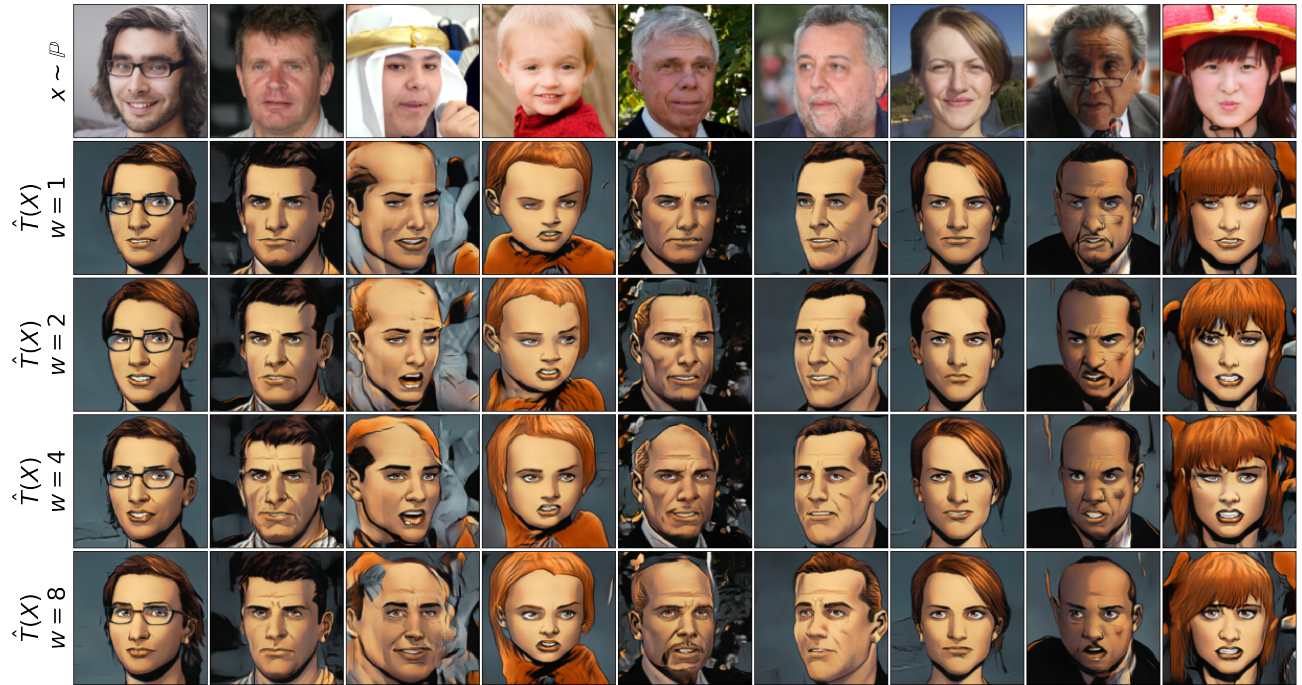

 Figure 20: *Celeba* (female) \rightarrow *anime* (64×64).

 Figure 21: *Handbag* \rightarrow *shoes* (128×128).


 Figure 22: *Textures* \rightarrow *chairs* (64×64).

 Figure 23: *Ffhq* \rightarrow *comics* (128×128).